UNIVERSIDAD DE CHILE
FACULTAD DE CIENCIAS QUÍMICAS Y FARMACÉUTICAS

"Specific isotope labeling of transthyretin for nuclear magnetic resonance and mass spectrometry studies"

(Marcaje isotópico específico de transtiretina para estudios en resonancia magnética nuclear y espectrometría de masas)

Memoria para optar al título de Bioquímico

Raúl Iván Campos Melo

Director de tesis:
Prof. Per Hammarström
The Department of Physics,
Chemistry and Biology
IFM, Linköping's University,
SE-581 83 Linköping,
Sweden

Profesor Patrocinante:
Dr. Dante Miranda Wilson
Departamento de Bioquímica y
Biología Molecular,
Facultad de Ciencias Químicas
y Farmacéuticas,
Universidad de Chile

Santiago de Chile, 2010

Dedicated to some of the most important people in my life:
my parents, my sisters and my Güeli.

ACKNOWLEDGEMENTS

TABLE OF CONTENTS

INDEX OF FIGURES

INDEX OF TABLES

ABBREVIATIONS

°C: Celsius degrees
1H: Hydrogen or proton
2D: Two-dimensional
2H: Deuterium
3D: Three-dimensional
AD: Alzheimer's disease
Amp: Ampicillin antibiotic
B: Effective magnetic field
B_0:   Externally applied magnetic field
B_1:   Oscillating radiofrequency
C_m: Concentration midpoint of urea denaturation
CNSA: Central nervous system amyloidosis
D_2O: Deuterated water
Da: Daltons
dH_2O: Distilled water
DNA: Deoxyribonucleic acid
E: Glutamic acid
EMR: Electromagnetic radiation
ESI: Electrospray ionization
F: Phenylalanine
FAC: Familial amyloid cardiomyopathy
FAP: Familial amyloid polyneuropathy
FID: Free induction decay
H: Histidine
HSQC: Heteronuclear single quantum coherence
HX: Hydrogen/deuterium exchange
HXMS: Hydrogen exchange mass spectrometry
IEC: Ion exchange chromatography
INEPT: Insensitive nuclei enhanced by polarization transfer
IPTG: Isopropylthiogalactoside
K: Lysine
K_d: Dissociation constant
kDa: Kilodaltons
K_{diss}:   Tetramer dissociation constant
L: Leucine
LB: Lysogeny broth
LC-MS: High performance liquid chromatography mass spectrometry
M: Bulk magnetization
M: Methionine
MALDI: Matrix-assisted laser desorption ionization
MALDI-TOF: Matrix-assisted laser desorption ionization time-of-flight

MilliQ:	Purified deionized water
MS:	Mass spectrometry
MW:	Molecular weight
MWCO:	Molecular weight cut-off
N:	Asparagine
Nm:	Nanometers
NMR:	Nuclear magnetic resonance
MTT:	(3-(4,5-Dimethylthiazol-2-yl)-2,5-diphenyltetrazolium bromide
OD:	Optical density
PBS:	Phosphate buffered saline
Ppm:	Parts per million
RBP:	Retinol binding protein
RF:	Radiofrequency
RPM:	Revolutions per minute
RT:	Room temperature (22°C)
S:	Spin angular momentum
SDS:	Sodium dodecyl sulfate
SDS-PAGE:	Sodium dodecyl sulfate polyacrylamide gel electrophoresis
SSA:	Senile systemic amyloidosis
T:	Threonine
T_4:	Thyroxine
TBS:	Tris buffered saline
TFA:	Trifluoroacetic acid
TOF:	Time of flight
Trp:	Tryptophan
TTR:	Transthyretin
UV:	Ultra violet
V:	Valine
Wt-TTR:	Wild type transthyretin
ΔE:	Energy difference or energy gap

ABSTRACT

Proteins are versatile molecules that play a variety of roles in maintaining the human body, e.g. transport of nutrients. Transthyretin (TTR) is a 55 kDa homotetrameric protein found in human plasma and in the brain, responsible for the transport of retinol (vitamin A) and T_4 (thyroxine). This protein is probably not essential for life, since TTR knockout mice have normal fetal development and lifespan. TTR, like 25 other human proteins, has been associated to the deposition of amyloid aggregates. Previous research has shown that mutations considerably increase the propensity of the protein to form aggregates. However, the wild type protein (wt-TTR) also exhibits this ability to aggregate, giving rise to the senile systemic amyloidosis disease that affects 20% people over 80 years of age. It is well accepted at the moment that self association of monomeric subunits triggers the disease through tetramer dissociation, since stabilization of the quaternary structure suppresses aggregate formation. Recently, our group discovered that wt-TTR purified at 4°C is just as toxic to human neuroblastoma cells as the most toxic small molecular weight aggregates, while when purified at room temperature (22°C; RT) it is not. Strikingly, this cytotoxicity was exhibited by the protein as a tetramer. Biophysical studies revealed a slight rearrangement of the tertiary structure of the protein. It is of high interest whether this minor structural change can lead to the discovery of new cytotoxic epitopes. Herein, we explored the protein structure in more detail by biophysical methods to confirm the existence of this conformational change and attempt to resolve where it specifically takes place in the protein structure.

Recombinant wt-TTR was expressed in *Escherichia coli* and purified by ion exchange chromatography and size exclusion chromatography at 4°C and RT. We studied the tetramer's intrinsic tryptophan fluorescence to confirm that cold purified and stored wt-TTR has a lower activation barrier for dissociation into monomers compared to the protein purified and stored at RT. This was performed by submitting the protein to unfolding using a high concentration of urea (6 M) as the chaotropic agent. We also carried out a hydrogen/deuterium isotope exchange mass spectrometry (HXMS)

experiment in order to study the local exchange of backbone amide hydrogens, which serve as probes for increased/decreased protection of different segments of the protein towards exchange, depending on the temperature. At last, nuclear magnetic resonance spectroscopy using the heteronuclear single quantum coherence (HSQC) experiment probing a ^{15}N isotope labeled wt-TTR grown in ~99% deuterated water M9 medium, allowed us to track the two dimensional ^{15}N-^{1}H J-coupling spectrum of the protein. Analysis of 2D spectra run at both temperatures revealed that some residues experience a clear change in chemical shift, indicating that changes in tertiary structure occurred. In conclusion, we determined that wt-TTR undergoes a conformational rearrangement when purified and stored at 4°C, although the exact location of this conformational change in the protein structure remains unclear.

RESUMEN

Las proteínas son moléculas versátiles que juegan una variedad de roles en la mantención del cuerpo humano, tal como el transporte de nutrientes. La transtiretina (TTR) es una proteína homotetramérica de 55 kDa que se encuentra en el plasma humano y en el cerebro, la cual es responsable del transporte de retinol (vitamina A) y T_4 (tiroxina). Sin embargo, probablemente no es necesaria para la vida, puesto que ratones *knock out* tienen un desarrollo fetal y longevidad normales. La transtiretina, al igual que otras 25 proteínas humanas, ha sido asociada a la deposición de agregados amiloides. Algunas investigaciones anteriores han mostrado que las mutaciones incrementan considerablemente la tendencia de la proteína a formar agregados. A pesar de esto, la proteína *wild type* (wt-TTR) también muestra la capacidad para agregarse. Esto genera la enfermedad llamada amiloidosis sistémica senil, la cual afecta a 20% de las personas sobre los 80 años de edad. Es sabido que la asociación entre subunidades monoméricas gatilla la enfermedad a través de la disociación del tetrámero, puesto que la estabilización de la estructura cuaternaria suprime la formación de agregados. Recientemente nuestro grupo descubrió que la wt-TTR purificada a 4°C es tan tóxica como los agregados de bajo peso molecular más tóxicos para células de neuroblastoma humanas, sin embargo no lo es cuando se purifica a temperatura ambiente (22°C; RT). Para nuestro asombro, esta actividad citotóxica era inducida por la proteína en su forma tetramérica. Estudios biofísicos revelaron un ligero reordenamiento de la estructura terciaria de la proteína. Es de especial interés si este pequeño cambio estructural puede conducir al descubrimiento de nuevos epítopes citotóxicos. En este trabajo exploramos la estructura proteica en más detalle mediante métodos biofísicos para confirmar la existencia de este cambio conformacional e intentar encontrar dónde específicamente ocurre en la estructura de la proteína.

Expresamos wt-TTR recombinante en *Escherichia coli* y la purificamos mediante cromatografía de intercambio iónico y cromatografía por exclusión de tamaño a 4°C y a RT. Estudiamos la fluorescencia intrínseca de triptófano de la proteína tetramérica para confirmar que wt-TTR purificada y almacenada en frío tiene una

menor barrera de activación para la disociación a monómeros comparado con la proteína purificada y almacenada a RT. Esto fue llevado a cabo mediante el desplegamiento de la estructura usando una alta concentración de urea (6,0 M) como agente caotrópico. También realizamos un experimento de intercambio isotópico de hidrógeno y deuterio con espectrometría de masas (HXMS) con el objetivo de estudiar el intercambio local de hidrógenos en los grupos amida del esqueleto polipeptídico, los cuales permiten medir el aumento/disminución de la protección de diferentes segmentos de la proteína en cuanto al intercambio, dependiendo de la temperatura. Por último, un experimento de resonancia magnética nuclear (NMR) llamado correlación heteronuclear de cuanto sencillo (HSQC), poniendo a prueba wt-TTR marcada con el isótopo ^{15}N cultivada en un medio M9 con agua deuterada al ~99%, nos permitió seguir el espectro de acoplamiento-J bidimensional entre ^{15}N-^{1}H de la proteína. El análisis de los espectros bidimensionales obtenidos a ambas temperaturas reveló que algunos residuos experimentan un claro cambio en su desplazamiento químico, indicando que efectivamente ocurren cambios en la estructura terciaria de la proteína. En conclusión, determinamos que wt-TTR sufre un cambio conformacional cuando es purificada a 4°C, a pesar de que la localización específica de éste en la estructura proteica continúa siendo desconocida.

1.- INTRODUCTION

1.1.- Proteins

Proteins are versatile molecules responsible for most of the reactions occurring in the human body such as transport of nutrients and oxygen, immune response, control of gene expression, catalysis, etc. The fundamental constituents of proteins are the amino acids, out from which 21 types are used to build proteins. A protein is usually composed of hundreds of amino acids bonded together by a peptide bond. It is the order in which these building blocks stick together that determines the final protein structure. This final structure is defined by different types of secondary structures called α-helixes and β-sheets and how these arrange among each other [1]. This secondary ordering or conformation determines the tertiary structure of a protein, which defines amino acid side chain interactions, and therefore protein function. A unique substitution of one amino acid for another can in some cases trigger a whole reordering of the structure and induce changes in the behavior of a protein, e.g., changes in the stability of the protein towards a denaturant or different pHs [2].

Proteins can interact among each other, which is necessary for many biological functions. These interactions can be transient, such as during intracellular signaling, or stable, like when they form complexes that can be structural (e.g. cytoskeletal proteins) or harmful (e.g. amyloid fibril formation) to the organism.

1.1.1.- Protein folding
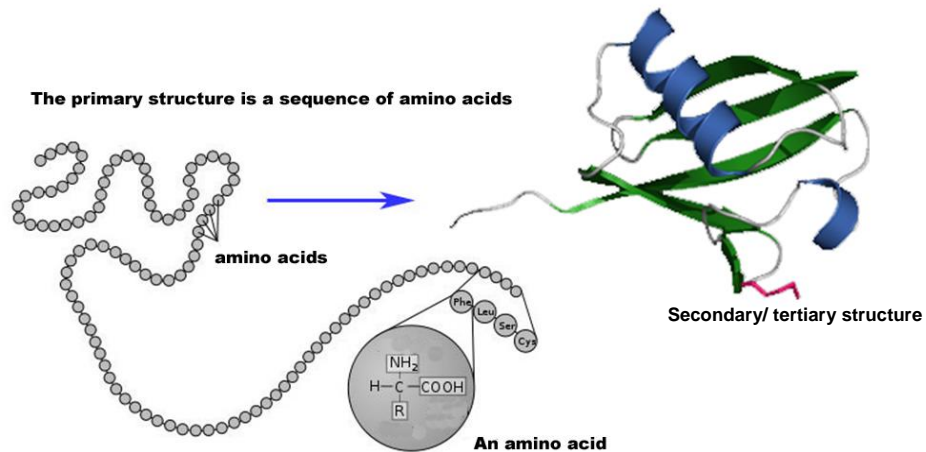
Figure 1: Schematic image of the primary structure of a protein showing the amino acids like a pearl necklace. The side chains of the amino acids, denoted with R, can be polar, non polar or charged. Groups of amino acids build up to form secondary structures such as α-helixes (blue) and β-strands (green). The latter interact through hydrogen bonds to form a β-sheet (green).

The normal protein function is not attained until the polypeptide develops its final three dimensional conformation, or in other words, when the protein has folded. Protein folding involves interactions among amino acids within the polypeptide to form the secondary structures, and through side chain interactions shape the final tertiary structure (Figure 1).   Folding takes place just after the polypeptide has been synthesized and is likely a fast process that can happen in a milli or micro second timescale for small proteins and takes several minutes for larger proteins.   The American biochemist Christian Anfinsen was the first scientist to demonstrate that the order of the amino acid sequence is the one that determines the final protein conformation. Moreover, he also found that if a folded protein is denatured, i.e. the hydrogen bonds, disulfide bonds, opposite charge interactions, hydrophobic interactions are disrupted and the protein unfolds, it is possible to refold it to its native conformation in appropriate chemical environment [1]. In spite of this, for many proteins the process described by Anfinsen is not so simple [3].   Folding takes place in the complex intracellular environment where only well folded proteins are stable in the long term and

are capable of selectively interacting with their natural companions. Being so, it should not be surprising that the lack of correct folding gives rise to a broad variety of pathological conditions. As a consequence, living organisms have developed a series of strategies to prevent this behavior. Of special interest is a system of proteins called "molecular chaperones", which is well preserved throughout evolution and is present in all cell types. The main function of the chaperones is to aid the correct folding of polypeptides. They are necessary to prevent aggregation and misfolding of a new chain [2]. Nevertheless, under certain pathological conditions the capacity of these control mechanisms is overwhelmed, giving rise to misfolding and diseases due to incorrect protein folding [4].

1.1.2.- Incorrect protein folding

Diseases due to incorrect protein folding are a wide range of human pathologies which has as its source the incapacity of a protein to adopt or maintain its native structure [5]. Among these we can mention some triggered by a loss of function, e.g. cystic fibrosis, hemophilia and cancer. Other diseases are caused by a mechanism through which the protein acquires toxicity, classically because of misfolded proteins that then start aggregating with each other, called amyloidosis (including the deposition of proteins in the form of plaques or amyloid fibrils) [4, 6]. This broad group is constituted by diseases caused by protein aggregates that misfold and deposite in tissues in the body. The reasons why they misfold could be mutations in the genes that code for these proteins or other factors such as stress. In some cases it is unknown why misfolding is triggered, which can have serious consequences for the cell and the organism in general. The amyloidosis include some of the most scary and expensive pathologies in the world. One of the first diseases of this kind was described in 1906 when the German neurologist Alois Alzheimer found a type of amyloidosis that affects the brain, which would be later called Alzheimer's disease (AD) [4, 7]. It is currently estimated that 24 million victims of AD exist worldwide [8]. In the fifties, the first form of transmissible human amyloidosis, called "Kuru", was found among groups that practiced cannibalistic rituals in Papua, New Guinea. Shortly after, a disease with a

similar pathology was discovered in Europe and United States; the transmissible spongiform encephalopathy, which spreaded out among patients treated with growth hormone extracted from human corpses. This disease includes the bovine spongiform encephalopathy or "mad cow disease" and Creutzfeldt Jakob disease, among others. Misfolded proteins called prions are implicated in these diseases [4]. It is currently debated whether these diseases are due to a loss of function or a gain in toxicity. Despite this fact, it is known that the infective species corresponds to misfolded oligomers of prion protein. In the classic amyloidosis, its specific associated protein is detected as an accumulation of fibrillar extracellular aggregates in different tissues depending on the disease type [6]; see Table 1.

Table 1: A selection of diseases coupled to protein misfolding and amyloidosis and their precursor proteins. Extracted and selected from ref. [9]	
Clinical syndrome	Fibril component
Alzheimer's disease	Aβ peptides (1-40, 1-41, 1-42, 1-43); Tau
Spongiform encephalopathies	Prion protein (full length or fragments)
Parkinson's disease	α-synuclein (wild type or mutant)
Senile systemic amyloidosis	Transthyretin (wild type or fragments)
Familial amyloidotic polyneuropathy I	Transthyretin mutant (over 45 variants or fragments)
Familial amyloidotic polyneuropathy III	Apolipoprotein A-1 (fragments)
Hemodialysis-related amyloidosis	β2-microglobulin
Type II diabetes	Pro-islet amyloid polypeptide (fragments)
Lysozyme systemic amyloidosis	Lysozyme (full length, mutant)
Insulin-related amyloid	Insulin (full-length)

1.1.3.- Amyloid fibril structure

All diseases caused by aberrant protein folding are characterized by the presence of fibrillar aggregates that are found as intracellular inclusions or extracellular plaques, constituted by a particular protein depending on the disease type (Table 1) [2, 9]. The peptides and proteins involved in amyloidosis do not have obvious similarities in terms of their size, amino acid sequence or structure. Nevertheless, the amyloid

fibrils that they convert into have striking similarities in terms of external morphology and internal structure, besides having an apparent similar assembly mechanism [10]. This process begins with a conformational change of the protein that then associates with identical protein molecules to generate aggregation nuclei for the formation of long unbranched fibers of 6-12 nm in diameter. These can form fibers up to several micrometers long that eventually accumulate in tissues or organs of the body with consequences from non symptomatic deposition to localized cell death or even loss of whole organ function [5, 9]. They are usually soluble and become insoluble and aggregate forming fibrillar structures (Figure 2) [11]. Strikingly, these fibers are very similar despite the differences between each precursor protein and consist of in-register parallel β-sheet type structures called cross-β-sheet that arrange perpendicular to the axis of the fibril [5, 9]. This makes them very stable, which can explain their insolubility and resistance to proteolysis [11]. This common structure that shapes the fibers is a common denominator and is believed to be responsible for binding of spectroscopic probes such as Congo red [11] and thioflavin T, among others [6]. Much evidence points out to that the principal component, besides the insoluble fibrillar deposits, are small soluble aggregates that are known as protofibers or oligomers of 2-5 nm diameter [9, 11, 12]. The properties of these oligomers are of increasing interest in order to understand in a better way the amyloid diseases and their development, especially since many studies have indicated that oligomers are the major toxic species when compared to mature fibrils [11, 13].
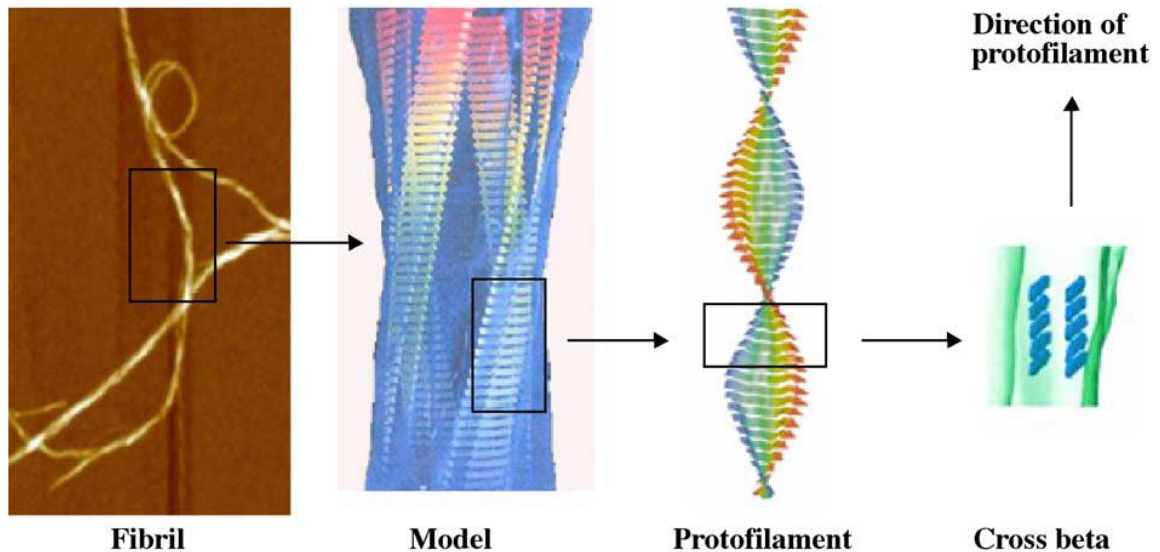
Figure 2: Close-up view of the structural organization of an amyloid fibril. Four protofilaments are wound around each other; their core structure is a row of β-sheets where each strand runs perpendicular to the fibril axis. Extracted from ref. [9].

1.2.- Transthyretin (TTR)

Alzheimer's and Creutzfeldt Jakob diseases are well known examples of amyloidosis. There are other similar pathologies that are less known but equally important such as the senile systemic amyloidosis (SSA), which is linked to the deposition of transthyretin (TTR) in its wild type form (wt-TTR) [14].

TTR was discovered in 1942 in the cerebrospinal fluid [15] and was first named prealbumin, because it migrated faster than albumin during electrophoresis. TTR was later identified in human plasma [16]. It is an abundant protein in extracellular fluids and binds the thyroid hormone T_4 (thyroxine). TTR is the only T_4 binding protein that is synthesized in the cells of the choroid plexus, a cell type comprising part of the blood brain barrier, producing the cerebrospinal fluid [17]. Hence TTR binds 80% of the central nervous system's T_4. At the plasma level it binds 15-20% of circulating T_4 [18]. TTR has a molecular weight of 55 kDa in its native state and its structure (studied by

crystallography and subsequent X-Ray diffraction) is a homotetramer with 4 identical monomeric subunits composed of 127 amino acids each (Figure 3) [18]. Each subunit has a molecular weight of 14 kDa and has eight β-strands, noted a-h (Figure 4), and an α-helix between strands e and f. The β-strands in each monomer form a β-barrel shaped by 2 groups of 4 anti-parallel β-strands that contain strands d, a, g, h and c, b, e, f. The association of two monomers forms a dimer called β-sandwich stabilized by hydrogen bonds between β-strands h-h' and f-f'. The association with another dimer is carried out via hydrophobic interactions among amino acids in the loops between the β strands a-b and g-h of each monomer. This association forms a tetramer with a central channel diameter of 8 Å and 50 Å long with 2 binding sites for T_4 that differ in their affinity. When one of the sites is occupied by a T_4 molecule, allosteric effects hinder a second T_4 molecule to bind to the other binding site (negative cooperativity). This
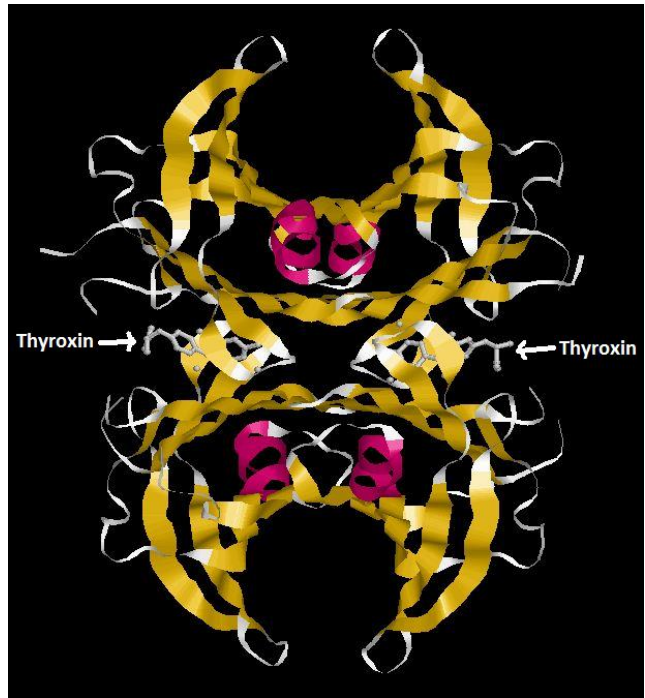
Figure 3: Rat tetrameric TTR. Thyroxine molecules (T_4) and their binding sites are indicated with arrows (www.pdb.org, pdb code: 1IE4).
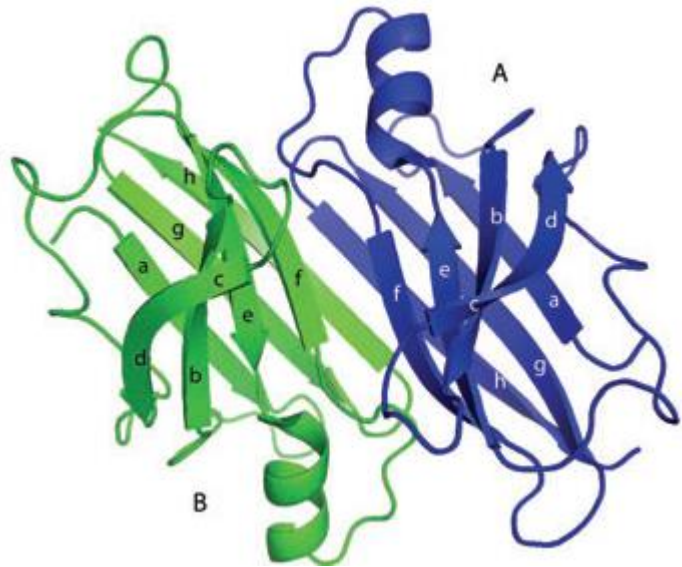
Figure 4: Two monomers, A and B, join side-by-side to form the dimer AB. The eight strands in each monomer are labeled a-h. Extracted from Ref. [16].

7

explains why only one of the binding sites is occupied in physiological conditions [16].

TTR is also involved in the transport of retinol (vitamin A) by forming a complex with the retinol binding protein (RBP), which is formed in the endoplasmic reticulum of hepatocytes and is released to the bloodstream after binding to retinol. If RBP is not bound to TTR it is quickly eliminated from plasma by glomerular filtration [18]. There are 4 binding sites to RBP, but only two can be occupied simultaneously due to steric limitations [16]. In the human plasma, the majority of TTR is not bound to RBP [17].

The three dimensional structure of TTR has been kept almost intact during vertebrate's evolution, with the exception of its N-terminal segment due to amino acid variations and deletions with implications for the T_4 binding affinity [16].

The origin of circulating plasma TTR is the liver. In the bloodstream TTR can be found at a concentration of 0,20 mg/mL (3.6 µM) [12], having a half life of 18-72 hours, which is rather short [19]. The TTR present in the cerebrospinal fluid is synthesized in the choroid plexus, with a circulating concentration of 0,02 mg/mL (0,29 µM) [12], from where it is known to escape to the bloodstream [16].

TTR is not likely to be essential for life, as TTR knockout mice have normal fetal development and a normal lifespan [17].

1.2.1- The model for TTR aggregate formation

TTR is one of the 25 human proteins, so far discovered, that have been associated to the deposition of amyloid aggregates [5]. Over one hundred mutations in the gene that codes for this protein have been reported so far and many of them are amyloidogenic [20, 21]. Several studies suggest that TTR amyloid disease begins when the tetramer dissociates into monomeric species that subsequently acquire an altered tertiary structure [20, 22, 23]. These non-native monomers are compact structures that can suffer structural changes that trigger the formation of aggregates and eventually amyloid fibrils, depending on their conformational stability (Figure 5) [20]. At the moment it is quite clear that TTR does not dissociate into stable dimer pairs, as determined by methods driving partial denaturation [19].
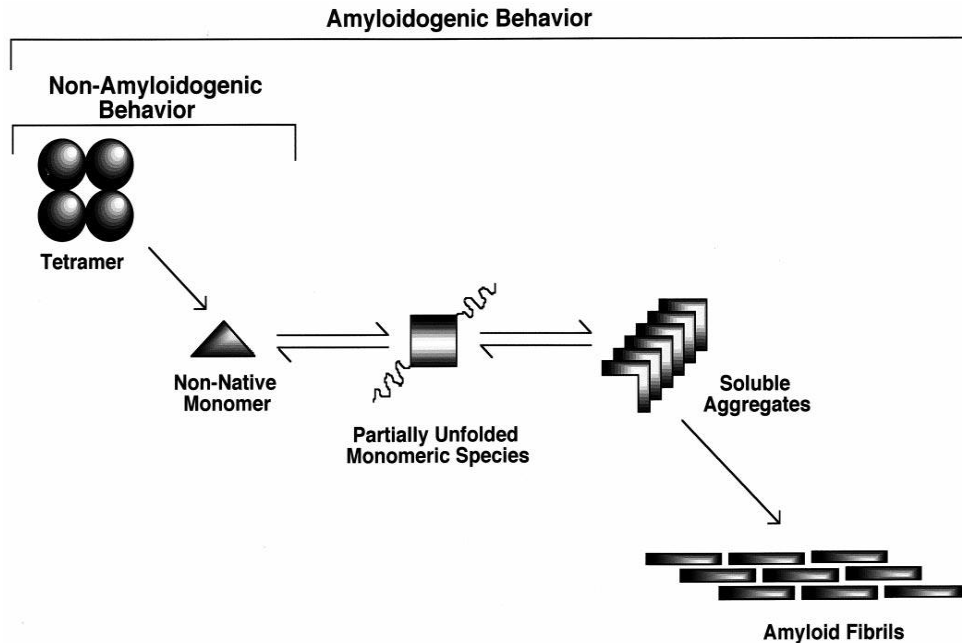
Figure 5: Model for amyloid fibril formation by TTR at commonly encountered physiological conditions. At 37° and pH 7, tetrameric TTR may dissociate to a non-native monomer, which in turn (depending on its conformational stability) may undergo partial unfolding that leads to aggregate formation and eventually amyloid fibril assembly. Extracted from ref. [20].

In vitro studies have unveiled that amyloidogenic and non-amyloidogenic variants of TTR can dissociate into non-native monomers, but the monomers of amyloidogenic variants have a lower conformational stability that primes them to form large amounts of monomeric species with partly unfolded structure. The presence of a critical amount of these species with aberrant structure appears to trigger the formation of amyloid deposits [20]. In support to this idea, many studies have corroborated that the main toxic species are monomers and low molecular weight oligomers [13, 18].

The question about how these conformational changes happen *in vivo* remains unanswered [5]. Several studies have demonstrated that amyloid fibrils are present proximal and inside lysosomes of reticuloendothelial cells of animals with amyloid disease [18]. A reasonable scenario for amyloid fibril formation in the lysosome is that aggregation-prone proteins are transported inside cells for degradation within lysosomes. The acidic chemical environment inside this organelle allows partial unfolding of these proteins, which end up as partly denatured monomeric species.

These species could potentially aggregate faster than the rate at which they can be degraded by proteolysis [18]. The acidic lysosomal pH favors the formation of amyloidogenic intermediates, despite the high stability of TTR as tetramers, which start forming at pH bellow 5 [18].

1.2.2.- TTR amyloid disease

The deposition of aggregates composed by wt-TTR and TTR variants is involved in several severe amyloidosis, such as familial amyloid polyneuropathy (FAP), familial amyloid cardiomyopathy (FAC), central nervous system amyloidosis (CNSA) and senile systemic amyloidosis (SSA) [12]. Over one hundred point mutations are associated to FAP, FAC or CNSA, which are characterized by amyloid deposits in the heart, peripheral nerves and the central nervous system, respectively [12]. FAP represents the most prevalent form of familial TTR amyloidosis. In the United States, the prevalence of TTR variants can reach up to 1 in 100.000 inhabitants [18], who start with the symptoms any moment from 20 years of age, losing their life after 5-15 years [24]. In affected individuals, mutant TTR has an altered folding that induces the formation of amyloid deposits in peripheral nerves, causing peripheral neuropathy [6] that is always progressive and fatal [25]. The V30M mutation is the most commonly associated FAP mutation, which is mainly found in Sweden, Japan and Portugal [14]. No effective treatment has been found against this disease other than liver transplantation, which replaces the mutant TTR secreting organ for a wt-TTR secreting one, resulting in disease regression [25], with the exception of an accelerated cardiomyopathy afterwards [24].

SSA is a common disease in the elderly population, once called senile cardiac amyloidosis, affecting 25% of the population over 80 years old. It is characterized by the deposition of amyloid fibers of wt-TTR in the heart. Since the wt form can also form aggregates, the primary sequence of the protein is not the only factor that triggers this amyloidosis. SSA is usually benign and asymptomatic. Some individuals, mainly men, are more severely affected with heavy deposits in the myocardium, sometimes giving

rise to cardiomegaly and congestive heart failure. The analysis of these amyloid deposits reveal that they are composed mainly by C-terminal TTR fragments starting from the positions 46, 49 and 52. It is tempting to speculate that proteolysis of the protein is the cause of the disease and that this could expose residues with a tendency to aggregate. However, the proteolysis mechanism is not known [14].

1.2.3.- Effect of decreased temperature in TTR cytotoxicity

A surprising finding was observed while wt-TTR cytotoxicity was assessed at different aggregation levels [13]. As expected, wt-TTR purified at room temperature (RT; 22°C) was not toxic for human neuroblastoma cells. However, in some controls cytotoxicity of wt-TTR was detected under native conditions. Going back carefully through the protocols, this was consistently associated with wt-TTR purification by gel filtration at a temperature of 4°C. Next, the cytotoxicity of native wt-TTR purified at this temperature was

Figure 6: TTR oligomers are cytotoxic.
A) Viability of human SH-SY5Y neuroblastoma cells measured by the MTT reduction test after 48 h exposure to vehicle (C), 20µM (on a monomer basis) native wt-TTR purified at 22°C and at 4 °C, or A-state wt-TTR aggregated for 5 min at 22°C. **B)** Analysis of native wt-TTR by native gel electrophoresis (pH 8,3) run at 4°C and at 37°C showing identical single band at both temperatures. The migration of reference proteins bovine serum albumin (BSA) and human carbonic anhydrase II (HCA II) are indicated with arrows. Extracted and selected from ref. [13].

tested by the MTT assay, which assesses cell survival, being similar to the toxicity of the most toxic amyloidogenic oligomers (Figure 6A). It was also proved that in native conditions the protein remained as a tetramer (Figure 6B) [13]. Experiments not yet published using small angle X-ray scattering, circular dichroism and tryptophan fluorescence have indicated a conformational change of the tetramer; however, there is no detailed information about the regions in the molecule where this conformational
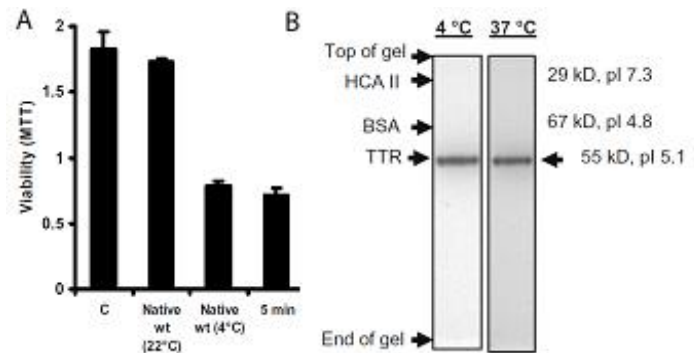
change takes place. It is known that TTR at 4°C compared to higher temperatures (25-37°C) is less resistant towards urea-induced denaturation [26] and that the rate of subunit exchange is significantly faster at 4°C [25]. The lower stability at lower temperatures, where the hydrophobic effect is weaker provides evidence that hydrophobic interactions play an important role in stabilizing tetrameric TTR. These hydrophobic interactions are evident in the crystal structure in that they contribute to both the edge-to-edge and face-to-face dimer interfaces stabilizing the quaternary structure [26]. The importance of this phenomenon has not been previously considered in terms of its biological or pathological relevance. It is possible that the conformation of TTR at 4°C displays a shielded c-b strand loop region indicative of a restrained loop conformation [13]. Our group has shown that early oligomers in the amyloidogenesis pathway of TTR have very high β-sheet content, even higher than native TTR [6]. For this reason and the fact that the cytotoxicity of wt-TTR is similar to the early oligomers, we speculate that these toxic conformations could be related in terms of exposed bio-active epitopes [13].

1.3.- Hydrogen Exchange Mass Spectrometry (HXMS)

While most biophysical techniques, such as circular dichroism, differential scanning calorimetry and ultra centrifugation, provide global information, X-ray crystallography and nuclear magnetic resonance (NMR) spectroscopy render localized, high-resolution structural information on proteins. However, the latter two techniques have limitations in applicability, sensibility and throughput. For crystallography, crystallization remains the major obstacle, as many proteins are inherently non-crystallizable. Most importantly, this technique only provides a static crystallizable state of a protein without giving any information about local dynamics. In the case of NMR spectroscopy, even with state-of-the-art high-field magnets, selective labeling methods, and new pulse sequences, some proteins are too large for analysis. In addition, the proteins are only studied under a limited set of conditions, e.g. in solid state in X-Ray crystallography and at high concentrations in NMR spectroscopy. Hydrogen exchange mass spectrometry (HXMS) fills a gap in the present set of biophysical tools where the

protein structure and dynamics can be analyzed under a wider range of experimental conditions [27].

The technique in short is based on the hydrogen exchange of the amide hydrogen in the peptide bond. In an exchange-in approach the undeuterated protein is incubated for defined intervals in a deuterated water environment, while in an exchange-out experiment a fully deuterated protein is incubated in a normal proton-containing buffer. After rapid quenching of the exchange reaction, the partially deuterated protein is enzymatically digested and the resulting peptide fragments are analyzed by a high performance liquid chromatography mass spectrometry (LC-MS) system. The deuterium incorporation of each peptic peptide fragment yields an average amide exchange rate that reflects the environment of the peptide in the intact protein [27].

Protein hydrogen atoms can be grouped according to their HX behavior. Hydrogens in the functional groups of the amino acid side chains ($-OH$, $-SH$, $-NH_2$, $-COOH$, and $-CONH_2$) and hydrogens from the amino and carboxy termini exhibit very rapid exchange. The exchange rates of these rapid exchanging hydrogens are too fast for the real-time measurement of in-solution HX. Another group includes carbon-bound aliphatic and aromatic hydrogens that do not participate in standard exchange reactions. These hydrogens will undergo isotope substitution only following activation by chemical treatment, such as reaction with hydroxyl radicals. A third group includes the backbone amide hydrogens of the polypeptide chain. In a folded protein, backbone amide HX rates are highly variable and can range over eight orders of magnitude. Because rates of backbone HX reflect the unique local environment of each amino acid in the three-dimensional (3D) structure, HX studies constitute a sensitive and unique method for protein structure analysis. As many main chain amide hydrogens in protein structures exchange over times ranging from seconds to days, the exchange kinetics can be readily followed in real time by stable isotope labeling. This is much slower compared to a random coil polypeptide, which typically exchanges within 10 to 1000 ms at room temperature and neutral pH. This is also called the "intrinsic exchange", and reflects experimental conditions such as pH and temperature [27].

1.4- Nuclear Magnetic Resonance (NMR) Spectroscopy

NMR spectroscopy is one of the most powerful techniques for the study of protein structure and dynamics [28]. Because it merely manipulates nuclear spins with very weak electromagnetic fields, NMR spectroscopy is virtually the only technique that provides atomic level information without disturbing the chemical properties of the molecules under investigation [29]. A brief summary of the fundamental background of this technique will be provided next, in order to explain how nuclear spins interact with a magnetic field (the chemical shift) and with each other (J-coupling and dipolar coupling) [30].

When a magnetic nucleus is placed in a magnetic field it adopts one of a small number of allowed orientations of different energies. For example, ^{1}H, ^{13}C and ^{15}N all have only two permitted orientations (Figure 7). Roughly speaking, the magnetic moment can point in the same direction of the field or against it. These states are separated by an energy difference or energy gap (ΔE) which depends on the magnetic moment (μ) of the nucleus and the strength of an externally applied magnetic field (B_0):

$$\Delta E = -\mu B_0 \qquad (1)$$

ΔE can be measured by applying electromagnetic radiation (EMR) at a certain frequency ν, which causes spins to flip from the lower energy level (pointing in the B_0 direction) to the upper one (pointing against the B_0 direction), provided the resonance condition

$$\Delta E = h\nu \qquad (2)$$

is satisfied (h is Planck's constant) [30].

Figure 7: Energy levels of a spin ½ nucleus in a magnetic field. The two permitted orientations of the nuclear magnetic moment relative to the magnetic field direction have energies differing by ΔE. Extracted from ref. [30].

Every nuclide has a characteristic μ, which would change the energy gap according to (1), which would make one think that if we apply an EMR at a frequency ν

we would flip all the nuclei of the same type. Fortunately for chemists, the resonance frequency also depends, slightly, on the chemical environment of the atom in the molecule, an effect known as "chemical shift". Basically, this means that when the atom is surrounded by a bigger electron cloud, the effective magnetic field (B) is lower than the externally applied one (B_0), the latter in other words being "shielded" [30].

The magnetic moment arises from the spin angular momentum (S) of the nucleus. S is quantized (as is all angular momentum) in units of $\hbar=h/2\pi$ and the different quantum states are indexed with the spin quantum number I. The total magnitude of the angular momentum is: $S=\hbar[I(I+1)]^{1/2}$. The spin quantum number I of a nucleus may have one of the following values:

I= 0, ½, 1, 3/2, 2, …

I depends on the number of unpaired protons and neutrons of each nuclei. For example, ^{1}H, ^{13}C and ^{15}N all have an I of ½ [30]. The present discussion will be centered on this type of nuclei since they are the most important for the following NMR spectroscopy experiment.

S is a vector quantity; its direction as well as its magnitude is quantized. The S vectors have just 2I+1 projections onto an arbitrary chosen axis, say the z axis. This is:

$I_z=m\hbar$

where m, the magnetic quantum number, has 2I+1 values in integral steps between +I and –I:

m=I, I-1, I-2, …-I+1, -I.

In other words, the S vector of a spin ½ nucleus such as ^{1}H, ^{13}C and ^{15}N has two permitted directions: +½$\hbar$ and -½$\hbar$ (Figure 8) [31].

The μ is also a vector quantity and is directly proportional

$+\tfrac{1}{2}\hbar$

$-\tfrac{1}{2}\hbar$

I = ½
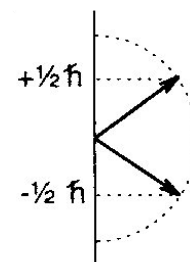
Figure 8: Space quantization of spin ½ nuclei. The S has magnitude $[I+(I+1)]1/2\hbar$ and z component m $\hbar$, where m is given by eq. 3. Extracted from ref. [30].

to S with a proportionality constant γ, known as the magnetogyric ratio:

$$\mu = \gamma S$$

γ depends on the type of nucleus (Table 2).

It is noteworthy that as mentioned above, the axis of quantization is arbitrary: in the absence of B_0, S and therefore μ have no preferred direction (Figure 9A) and all the directions have the same energy. However, once the spins are placed in a magnetic field, the magnetic moments assume two orientations, either in the same direction as, or opposed to, the magnetic field (Figure 9B) [32].

As stated before in eq. (1), the energy of the states depends on the interaction between the vectors μ and B_0, and more precisely, on minus the dot product of the μ vector and the B vector.

Figure 9: Orientation of nuclear magnetic moment (μ) in the absence (A) and in the presence (B) of an external magnetic field B_0. Extracted from ref. [31].

After some equation rearrangements we can show that the energy of the nucleus is shifted by an amount proportional to B, γ and the z component of S. This means that in order to produce a transition between the two adjacent energy levels we can meet the resonance condition in eq. (2), which will give us the well known Larmor equation:

$$\omega = \gamma B$$

ω [rad x s^{-1}] refers to the absorption or resonance frequency of the

Table 2: Magnetogyric ratios, NMR frequencies (in a 9,4 T field) and natural abundance of selected nuclides. Extracted from ref. [30].			
Nuclei	γ (rad x s^{-1} x $gauss^{-1}$)	v/MHz	Natural Abundance/%
^1H	26,753	400	99,99
^{13}C	6,728	101	1,11
^{15}N	-2,712	41	0,37

shielded nucleus, i.e. its observed resonance frequency [31].

Figure 10: At equilibrium, a sample has a net magnetization along the magnetic field direction (the z axis). Extracted from ref. [32].

The energy of an NMR transition is quite low, requiring radiofrequency (RF) waves to excite the spins. The small value of ΔE has two important consequences: the population difference between the two energy levels is quite small, on the order of 1 part in 10^6 [31], which makes NMR spectroscopy a relatively insensitive technique because of the small excess of spins in the ground state. The ratio of populations in the two levels is:

$$n_{upper}/n_{lower}=e^{-\Delta E kT}$$

where ΔE equals ħγB and k is the Boltzmann's constant [30]. The second important consequence is that the lifetime of the excited state is quite long, on the order of ms to s. This provides narrow resonance lines, allows for the manipulation of the sample in multidimensional experiments and also means that the experiment will be sensitive to molecular motions over a wide time scale [31].

Spectroscopy at higher frequencies is more sensitive because the high γ and therefore high energy protons are easier to detect. Therefore, it is important to use nuclei with high γ and have high B_0 in order to maximize the ΔE [30].

It is very convenient that instead of thinking on several magnetic moments precessing around the z axis (when an external B_0 is present), we think about net effect of all these nuclei when each contribution is added up, since in NMR we do not observe only one nucleus. This in other words is called the bulk magnetization (M) vector of the sample and in the thermal equilibrium it points towards the z axis (Figure 10) [32].

When one applies a small magnetic field, such as an oscillating RF (B_1), near the Larmour frequency (ω) along the xy plane (90° pulse), one will tilt the M to the xy plane (Figure 11). Conveniently we can use the same coil that we can use to generate this EMR to detect the oscillating current along a fixed axis in the xy plane [32].
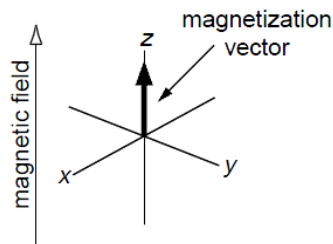
This detected signal, which will return with time to the z axis, is called the free induction decay (FID) and is the sum of all the oscillating voltages from the various nuclei in the sample, each with a characteristic chemical environment. It contains all the information necessary to obtain the NMR spectrum [30].

Figure 11: Effect of 90°x B_1 pulse on M. After the pulse is applied along the x axis at the selected resonance frequency, M changes direction from the z to the -y axis and then starts precessing on the xy plane.

The final step is to unravel all these oscillating components in the FID, which is a function of the time (Figure 12), to obtain a spectrum of NMR intensity as a function of frequency (ω). This is done by means of a Fourier transform [30]. This will give us single peaks for every characteristic nuclei.

The above description might have given the idea that the appearance of an NMR spectrum is determined solely by chemical shifts, but there is another extremely valuable source of information encoded in most NMR spectra, which is the magnetic interaction between nuclei connected by bonds called J-coupling.

Figure 12: A simple one pulse NMR experiment begins with a short (~10 µsec) radiofrequency pulse. The induced signal (FID) is sampled as it evolves over time. Extracted from ref. [32].

This interaction causes the peaks of a spin ½ nuclei to noticeably split when other spin ½ nuclei is no more than 3 bonds away, generating multiplets instead of a sharp single peak. NMR spectra are normally measured with one of the nuclei decoupled, which is achieved by irradiating the sample at the resonance RF of one of the nuclei while other is being recorded. Decoupling makes the multiplets collapse into 1 single peak. Decoupled spectra are less crowded and have higher sensitivity [30].

Another important interaction is called dipolar coupling, which arises from the fact that every spin ½ nuclei is a magnetic dipole. A magnetic nucleus behaves ike a small bar magnet with north and south poles. The most common way to depict this dipole is a plot of lines of force (Figure 13). As one can see, the magnitude and direction of the field depends on distance and the angle from the point where it is measured. Nevertheless, molecules in liquids rotate rapidly with frequent changes in the axis and speed of rotation as a result of collisions with other molecules, which is called molecular tumbling. Therefore, the

Figure 13: Lines of force representation of a dipolar magnetic field generated by a magnetic dipole pointing along the x axis. Extracted from ref. [30].

angle and the dipolar coupling become rapidly modulated. This leads to an average splitting, i.e. disappears, provided the frequency at which the coupling is modulated greatly exceeds the coupling itself. This condition is certainly met for all but very large molecules, viscous solutions or measurements at low temperature. Dipolar interactions do not therefore produce splitting in the NMR spectra of liquids: however they do play a crucial role in spin relaxation (process that makes the µ of all the different nuclei go back to the z axis after a RF pulse) [30]. However, in large slow tumbling proteins, dipole-dipole interactions may broaden lines beyond detection. Isotopic replacement of ^{1}H with ^{2}H can be used to reduce the dipole-dipole interactions among spin ½ nuclei [29].

Perhaps the most important set of NMR spectroscopy experiments are the two-dimensional (2D) which transfer magnetization from one spin to another via the J-coupling between them. This is very useful, since for example, the reduction in sensitivity is 300 fold less for ^{15}N compared to ^{1}H. Consequently, most heteronuclear NMR experiments are designed to transfer the intense spin polarization of the proton to the heteronuclear spin. The sensitivity of the experiment is increased further by

returning the magnetization back to the proton for detection at the end of the experiment. The sensitivity of these experiments can be further increased by decoupling the proton-heteronuclear interaction during periods of chemical shift evolution. Decoupling increases the signal by a factor of four for small proteins [31].

One particularly useful experiment is to record a 2D NMR spectrum in which the correlate of a peak in one dimension is the chemical shift of one type of nucleus (e.g. ^{1}H) and the co-ordinate in the other dimension is the chemical shift of another nucleus (e.g. ^{15}N) which is coupled to the first nucleus. The one-bond coupling between a ^{15}N and the proton directly attached to it is relatively constant (around 90 Hz), and much larger than any of the long-range ^{15}N-^{1}H couplings. By utilizing this large difference experiments can be devised which give maps of ^{15}N shifts vs the shifts of directly attached protons. Such spectra are very useful as aids to assignment (determining what part of the molecule originates what peak in the spectrum); for example, if the proton spectrum has already been assigned, simply recording a ^{15}N-^{1}H correlation experiment will give the assignment of all the protonated nitrogens [32].

Only one kind of nuclear species can be observed at a time, so there is a choice as to whether observe ^{15}N or ^{1}H when recording a 2D correlation spectrum. It is very advantageous from the sensitivity point of view to record protons because its higher NMR frequency induces a larger magnetization that produces higher voltage in the detector coil [31].

From the 2D correlation experiments, HSQC is probably the most used one in protein NMR spectroscopy. Each residue of the protein, besides proline, has an amide ^{1}H attached to the ^{15}N in the peptide bond. The number of peaks in the spectrum should approximate the number of residues in the protein, although the residues with sidechains with nitrogens attached to protons such as arginine, asparagine, histidine, lysine, glutamine and tryptophan will add additional peaks. The difficult process of structure determination is usually not performed until a good HSQC is obtained [31].

The pulse sequence (Figure 14) starts with a first period of polarization transfer, called Insensitive Nuclei Enhanced by Polarization Transfer (INEPT), from ^{1}H to ^{15}N to enable the spectroscopist to recorder the ^{15}N evolution (^{15}N spins' FID) with a higher sensitivity thanks to J-coupling. The INEPT element flips the ^{1}H M into the z axis while the ^{15}N M is transferred to the -y axis. So, during the evolution t_1 period there is no

evolution for ^{1}H spins, while one can record the ^{15}N FID. At half this period, a 180° x pulse flips the ^{1}H M down to the –z axis. The reverse INEPT sequence, which is the second INEPT element, brings polarization back to protons and allows the ^{1}H M to be flipped to the x axis, from where the ^{1}H FID can be recorded, while the ^{15}N M ends up in the z axis without interfering. During the detection period t_2, ^{15}N decoupling is applied so that only a single resonance line is detected for each ^{15}N-^{1}H pair [31].
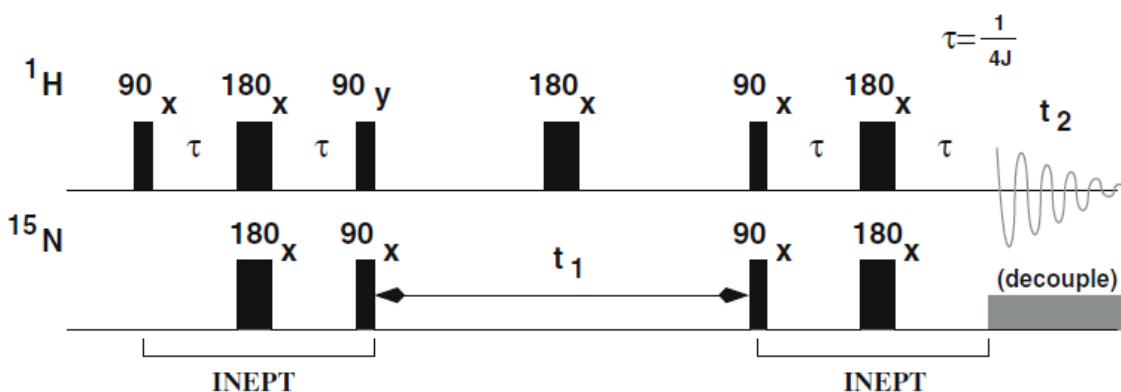
Figure 14: HSQC pulse sequence. The set of pulses are applied to the protons and the lower set of pulses are applied to the heteronuclear spins (^{15}N in this illustration) via a separate radio-frequency channel. Narrow bars correspond to 90° pulses and wider bars represent 180° pulses. The delay τ is nominally set to 1/4J (J is the single bond ^{15}N-^{1}H J-coupling constant). Polarization transfer periods (INEPT) are labeled, the second one being more specifically a reverse INEPT sequence. Extracted from ref. [31].

1.5.- Hypothesis

Using isotopic labeled wt-TTR in conjunction with nuclear magnetic resonance (NMR) and mass spectrometry (MS), crucial sites for the likely conformational change occurring in cold (4°C) wt-TTR *versus* room temperature (22°C) may be identified.

1.6.- General Objective

To study the conformational changes of TTR at room temperature (22 °C) and at low temperature (4 °C) using isotope labeled TTR and biophysical analyses with NMR and mass spectrometry.

1.7.- Specific objectives

1. Produce and purify unlabeled wt-TTR for studies of denaturation kinetics and HXMS.

2. Confirm the preparations show the previously observed difference in tetramer dissociation rates.

3. Produce and purify uniformly ^{15}N labeled wt-TTR for studies in liquid state NMR spectroscopy.

4. Study the structural differences of tetrameric TTR at room temperature and at low temperature using HXMS and NMR spectroscopy.

2.- MATERIALS AND METHODS

2.1.- Plasmid

The Pmm Hα plasmid containing the human TTR DNA sequence (obtained from Jeffery W. Kelly and David Wemmer) was sequenced (GATC Biotech, Konstanz, Germany) and the corresponding protein sequence was checked using the ExPASy Proteomics Server to confirm that the correct protein was expressed and analyzed, i.e. a methionine codon before wt-TTR sequence followed by a stop codon at the C-terminal end. Biophysical studies indicate that neither stability nor amyloid formation is affected by the presence of the N-terminal methionine [19]. This gave us a recombinant wt-TTR protein with an extra methionine residue in the N-terminal end and therefore a total of 128 amino acids:

```
    10     20     30     40     50     60
MGPTGTGESK CPLMVKVLDA VRGSPAINVA VHVFRKAADD TWEPFASGKT SESGELHGLT


    70     80     90    100    110    120
TEEEFVEGIY KVEIDTKSYW KALGISPFHE HAEVVFTAND SGPRRYTIAA LLSPYSYSTT


   128
AVVTNPKE
```

The theoretical molecular weight is 13892.6 g/mol and the corresponding extinction coefficient of 18450 $M^{-1}cm^{-1}$ was used for concentration determinations (http://au.expasy.org/tools/protparam.html).

2.2.- Transformation

Wt-TTR was to be expressed in BL21/DE3 *Escherichia coli* cells, following transformation with the Pmm Hα TTR plasmid. Transformation was performed using

electroporation (MicroPulser™, BIO-RAD) at 2.5 mV by mixing 50 µL fresh cells previously stored at -80°C with 2 µL plasmid stored at -20°C in an electroporation cuvette. The electroporation cuvette, cells and plasmid were kept in ice at all times to increase electroporation efficiency. Electroporation increases permeability of bacterial membrane by applying an external electrical field that creates temporal water filled pores. This allows cellular uptake of DNA, which is a large charged molecule that would not passively diffuse across the hydrophobic phospholipic bilayer core [33].

Right after electroporation, the cells are quickly mixed with 300 µL SOB medium (see Appendix) previously warmed up to 37°C and incubated 1 hour at 37°C before transferring to Lysogeny Broth (LB) agar plates (see Appendix) with 100 µg/mL Ampicillin Sodium (Amp) (Duchefa Biochemie, Haarlem, The Netherlands). The Pmm Hα plasmid contains an Amp resistance gene that allows only those cells that actually acquired the plasmid during the electroporation to survive. This is because the gene codes for the β-lactamase enzyme which deactivativates Amp's transpeptidase competitive inhibitory action during cell wall synthesis needed for bacterial binary fission.

2.3.- Protein expression for Hydrogen Exchange Mass Spectrometry (HXMS) and urea unfolding studies

BL21/DE3 *E. coli* cells that acquired the plasmid grew on the plates and a single colony was picked with a pipette tip and transferred to a 15 mL LB medium (see Appendix) with 100 µg/mL Amp at 37°C and incubated with shaking for aprox. 12 hrs. This culture was then transferred to a 1,5 L LB medium with 100 µg/mL Amp and incubated again at 37°C with shaking and grown until the optical density at 660 nm (OD_{660}) reached over 1. This was usually achieved after 6 hours. Then, through the addition of isopropylthiogalactoside (IPTG) to a concentration of 1 mM, protein expression is induced. This bacterial strain contains a gene coding for the T7 RNA polymerase which is controlled by the lac operon through the lac repressor protein.

When IPTG is added, a conformational change is induced in the repressor protein which represses its binding to DNA with subsequent transcription of the T7 RNA polymerase. Once this protein is translated, it binds to the T7 promoter sequence in the plasmid and the expression of the protein of interest begins. Using this system, target protein expression can be regulated. The culture is left under induction for 5 hours at 37°C before harvesting cells.

Cells are harvested by centrifugation at 2500g during 45 minutes at 4°C using a Z513K Hermle centrifuge. Then the supernatant is removed and the pelleted cells are resuspended by vortexing with TBS (Tris-HCl 20 mM, NaCl 0,5 M, pH 7,5), using 100 mL per liter of culture. Finally, the resuspended pellet is frozen over night at -80°C.

2.4.- Verification of protein expression by sodium dodecyl sulfate polyacrylamide gel electrophoresis (SDS-PAGE)

500 µL samples from the LB growth media taken before IPTG addition and just before harvesting are used for protein expression assessment. These samples are centrifuged 10 minutes at 13000 RPM before resuspending the pellet with 100 µL dH_2O and adding 25 µL SDS cocktail (see Appendix). Then the samples are boiled for 5 minutes before loading 20 µL from each sample to gel wells for sodium dodecyl sulfate polyacrylamide gel electrophoresis (SDS-PAGE).

In SDS-PAGE, proteins are separated according to their electrophoretic mobility, which depends on their molecular weight, since the negatively charged SDS binds to the proteins with a stoichiometry of around one molecule every two residues and destroys all non-covalent bindings. This results in proteins with the same shape and with negative charges in proportion to their mass. The gel where the proteins are loaded consists of a network of pores built up by polyacrylamide where an electric current is applied. The proteins will then migrate in the gel towards the anode (positive)

and the rate of migration will only depend on their molecular weight. Smaller proteins will migrate faster than the rest, the latter needing longer time to migrate. The gel consists of two parts: first, the stacking gel (which in this case has 4% acrylamide), with large pores, which will ensure that the proteins start migrating together through the separation gel (which in this case has a 15% acrylamide content), with smaller pores, which will separate the protein according to their size (See Appendix for gel recipes). For molecular weight reference one well of the gel was loaded with 5 μL Precision Plus Protein™ Dual Color Standards (BIO-RAD) and another one with PageRuler™ Prestained Protein Ladder (Fermentas Life Sciences), which contains a mixture of proteins with known molecular weights (250, 150, 100, 75, 50, 37, 25, 20, 15 and 10 kD for the former and 170, 130, 95, 72, 55, 43, 34, 26, 17 and 10 kD for the latter). SDS buffer (see Appendix) was used as running buffer. The electrophoresis was first run at 100 Volts (V) for 30 minutes and then at 180 V until the front blue line (bromo phenyl blue marker) reached the end of the gel.

After SDS-PAGE, gels were stained using Coomassie Brilliant Blue R-250 (DBH, England) solution for 1 hour and destained during 4 hours using destaining solution several times to increase contrast. Gels were stored in gel storing solution (See Appendix for solution's recipes) and pictures were taken for the record.

2.5.- Protein purification

Cells containing the expressed protein were thawed in a warm water bath (~30°C) and sonicated, using a BRANSON Digital Sonifier®, 4 times for 30 seconds with 1 minute resting intervals between cycles to disrupt cell membranes and release their content. Cells were kept on ice at all times to avoid heating. Afterwards, cell debris was pelleted by centrifugation at 7000g for 15 minutes using a SIGMA 3-18K centrifuge. The resulting supernatant was then submitted to a single 0-50% NH_4SO_4 salting in cut to discard unwanted proteins that have a lower solubility than TTR. The corresponding amount of NH_4SO_4 is added according to:

(Amount of NH$_4$SO$_4$ to add) = (Supernatant volume) x (291 g NH$_4$SO$_4$)/(1 L)

This is done at room temperature by slowly adding the chemical and stirring fo
up to 15 minutes to dissolve all the salt. Then the precipitated proteins are discarded
after centrifugation at 7000g for 15 min. Next, the supernatant is filtered through 0,4!
µm filters and dialyzed over night against 8 L of Tris-HCl 25mM pH 8 using
Spectra/Por® dialysis membranes (Spectrum Laboratories, Inc., CA, USA) with a
12000-14000 molecular weight cut-off (MWCO) in order to eliminate the salts from the
protein solution. The next day, the dialyzed protein is concentrated up to 20 mg/mL
before injecting it in an ion exchange chromatography column.

Ion exchange chromatography (IEC) followed by gel filtration was used to further
purify wt-TTR. IEC is a form of adsorption chromatography which separates molecules
on the basis of their charge. Separation in ion exchange chromatography depends upon
the reversible adsorption of charged solute molecules to coupled ion exchange groups
of opposite charge. The technique is capable of separating molecular species that
have only minor differences in their charge properties, for example two proteins differing
by one charged amino acid. The base matrix of the column is highly cross-linked
agarose which gives the anion exchanger high chemical and physical stability. This
means that characteristics such as capacity, elution behavior and pressure/flow rate are
unaffected by the solutions commonly used in process chromatography and cleaning
procedures. IEC was carried out at 4°C using a Q Sepharose Fast Flow column (GE
Healthcare Bio-Sciences AB, Uppsala, Sweden) which is a strong anion exchanger.
The anion exchange group is a quaternary amine group:

-O-CH$_2$CHOHCH$_2$OCH$_2$CHOHCH$_2$N+(CH$_3$)$_3$
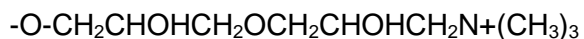
The column was equilibrated with Tris-HCl 25 mM pH 8 and a gradient up to
35% of a buffer that contains Tris-HCl 25 mM, NaCl 1 M pH 8 with the objective of
eluting wt-TTR due to the gradual increase in ionic strength, which can be traced with a
conductivity detector connected to the BioLogic LP (BIO-RAD) pump connected to the
columns. The protein elutes at the end of the gradient, which can be traced using a 280
nm absorption wavelength UV lamp connected to the pump that allows to determine

which elution fractions correspond to the peak in protein absorption during the last part of the gradient. The presence of wt-TTR is further verified taking a 100 µL sample from each selected eluted fraction, which was mixed with 25 µL SDS cocktail and boiled for 5 minutes to run a SDS-PAGE followed by Coomassie staining, a process which was described in section 2.4. Then, the protein is concentrated up to 10 mg/mL using several Centriprep Ultracel YM-10 (MILLIPORE) regenerated cellulose centrifugal tubes with a 10.000 MWCO and centrifugation at 3.000 x g using a SIGMA 3-18K centrifuge.

The second column purification step is carried out either using a HiLoad Superdex™ 75 16/60 (GE Healthcare Bio-Sciences AB, Uppsala, Sweden) gel filtration column at 4°C or with a Superdex™ 75 HR 10/30 for the wt-TTR purified at RT. The columns were equilibrated with autoclaved and filtered 50 mM Na_2HPO_4, 100 mM NaCl buffer adjusted to pH 7,5 with concentrated HCl. The gel filtration columns are composed of a composite matrix of dextran and highly cross-linked agarose. Gel filtration is a liquid chromatography technique that separates molecules according to their size. It is sometimes called size exclusion or gel permeation chromatography. This allows one to select the native wt-TTR peak using the UV lamp to select the correct eluted fractions. The wt-TTR absorption peak can be seen at around 1/4 the bed volume (~45 mL for the 4°C column and ~13 mL for the RT purification column). The presence of wt-TTR is further verified taking a 100 µL sample from each selected eluted fraction, which again were mixed with 25 µL SDS cocktail and boiled for 5 minutes to run a SDS-PAGE followed by Coomassie staining, as described in section 2.4. Finally, the selected wt-TTR eluted fractions are mixed and concentrated up to ~4 mg/mL using several Centriprep Ultracel YM-10 (MILLIPORE) regenerated cellulose centrifugal tubes with a 10.000 MWCO and centrifugation at 3.000 x g using a SIGMA 3-18K centrifuge.

2.6.- Protein confirmation using matrix-assisted laser desorption ionization time-of-flight (MALDI-TOF) mass spectrometry

In order to assess the integrity of the protein sample, we ran a MALDI-TOF mass spectrometry analysis using a Voyager-DE™ STR MALDI (PerSeptive Biosystems, Framingham, MA) mass spectrometer equipped with a Nitrogen 337 nm laser. MALDI is the name of the strategy used to ionize the protein sample, which is mixed with a low molecular weight UV absorbing matrix. This matrix enhances protein ionization; when the laser shoots the sample, it goes to gas phase as ionized single molecules. A variable voltage grid fine-tunes the ions' acceleration (Figure 15). In this case, we used sinapinic acid (MW= 224.07 Da) as matrix, which is recommended for protein samples >10.000 Da. So, a small volume of the concentrated protein was diluted to 10 pmol/µL and mixed 1:1 with 10 mg/mL sinapinic acid in 70% acetonitrile and 0,3% trifluoroacetic acid (TFA). Then, a 1,3 µL volume from this mixture is placed and let dry on a steel MALDI plate. The final protein concentration in the plate was 5 ~pmol/µL, which is in the recommended 0,1-10 pmol/µL concentration range for protein samples. The plate was supplied with 20.000 V to accelerate the ions into the flight tube. This field-free tube together with the beam guide wire
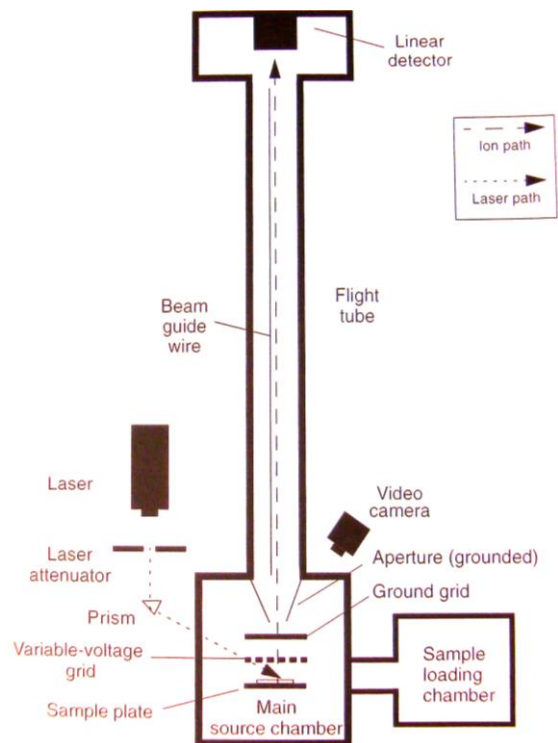

Figure 15: Parts of a Voyager-DE Biospectrometry Workstation. Extracted from ref. [34]

make ions fly at a velocity inversely proportional to the square root of their masses. Therefore, ions of the same mass will hit the detector at the same time giving rise to sharper peaks. A TOF mass analyzer is used to separate and detect the ions formed. A linear detector measures ions abundance over time and sends a signal to the digitizer for conversion. Mass accuracy is over 0.05% for myoglobin (16,953 kDa), with external calibration [34, 35]. Each mass spectrum was normalized with respect to its maximum intensity.

2.7.- ^{15}N labeled wt-TTR expression in deuterated medium (D$_2$O) for NMR studies

An identical procedure of transformation, plate culturing and colony selection, as described in sections 2.2 and 2.3 was performed for this preparation starting with 15 mL LB medium containing 100 µg/mL Amp. In this case we followed a modified protocol described by Lundström *et al* [36] for the expression of deuterated wt-TTR with ^{15}N labeling with an occupancy level of ~99% (all nitrogens and hydrogens of the molecule in isotopic form). The 15 mL starting cell culture was centrifuged at 3000g for 30 minutes and sufficient pellet resuspended in 100 mL ^{15}N D$_2$O M9 medium with 100 µL of added LB medium (see Appendix) with 1 µg/mL carbenicillin instead of Amp, to achieve a starting OD$_{660}$ of 0,1. This was incubated at 37°C. The source of ^{15}N label is ^{15}NH$_4$Cl, which is included in the D$_2$O M9 growth medium.

Carbenicillin, which only differs from Amp in a functional group of the molecule, is used instead because it is more stable than Amp during long growing times [37]. The M9 deuterated medium needed to be incubated 2-3 times longer than a protonated M9 medium in order to achieve the desired final OD.

After the 100 mL ^{15}N D$_2$O M9 medium reached an OD$_{660}$ of 1, it was transferred to a 900 mL ^{15}N D$_2$O M9 medium. When the OD$_{660}$ of this 1 L ^{15}N D$_2$O M9 medium reached 0,6, IPTG was added to a final concentration of 1 mM to induce plasmid expression. Cells were harvested in an identical way as described in section 2.3.

Purification and protein assessment was performed as described for unlabelled wt-TTR in sections 2.4, 2.5 and 2.6. For this protein preparation, 0,005 g/L sodium azide was added to the 50 mM Na_2HPO_4, 100 mM NaCl pH 7,5 buffer in order to keep the samples free from bacterial contamination.

2.8.- Urea denaturation kinetics derived from Trp fluorescence

Denaturation as a function of time was studied for wt-TTR 0,1 mg/mL (7,2 μM), purified and stored at RT or 4°C. This was carried out in order to corroborate previous results with the current preparations. In the previous study, the stability as a function of increased urea concentration showed differences depending on the temperature the protein was purified and incubated at [26]. All wt-TTR Trp fluorescence spectra were recorded over the range of 310-400 nm using a F-4500 Fluorescence Spectrophotometer (HITACHI) equipped with a thermostated cuvette holder employing excitation at 295 nm in order to excite only tryptophan residues [20]. Native wt-TTR exhibits a fluorescence maximum at 337-338 nm, whereas the unfolded protein shows a maximum emission between 355 and 358 nm. Each subunit of TTR has two tryptophan residues at positions 41 and 79. We used the 355 nm:335 nm emission intensity ratio to follow denaturation by exposure of the tryptophans as a function of time. A 10 mM Na-phosphate 100 mM KCl 1mM EDTA and 1 mM DTT pH 7,5 buffer with a urea concentration of 6,0 M was used, which is two times the midpoint of urea denaturation (C_m) determined before (3,2 ±0,04) for the more stable 25°C wt-TTR [38]. The kinetic data fit well to a single exponential function: $I^{355/335} = I_N^{355/335} + A(1-e^{-k_{diss}t})$, where $I_N^{355/335}$ is the native protein fluorescence intensity ratio (355 nm/335 nm), A is the amplitude difference, k_{diss} is the tetramer dissociation rate constant, and t is time in hours [46]. The ratio increased from 0,85 to 1,11 after 94 hrs for the RT sample and from 0,84 ± 0,01 (done by triplicate) to 1,25 for the 4°C sample. This is very similar to the 0,85 ± 0,02 starting ratio obtained in the previous study, although the final pH in

those experiments was 7,0 [26]. In the same study the spectrum of a solution of free tryptophan in the same buffer displayed a ratio of 1,4. The unfolding was recorded over a period of 4 days, which is enough to reach equilibrium [38].

A temperature jump experiment was also carried out in order to determine the inflexion point in the denaturation curve due to a change of structure triggered by the temperature. In order to do this, each protein sample at its corresponding temperature was diluted ~50 fold in 6 M urea buffer, which was pre-equilibrated at either RT for the 4°C protein sample or 4°C for the RT protein sample. Then the solution was vortexed and the change of fluorescence ratio measured with a dead time of ~1 minute for protein dilution before the start of data collection.

2.9.- Hydrogen Exchange Mass Spectrometry (HXMS)

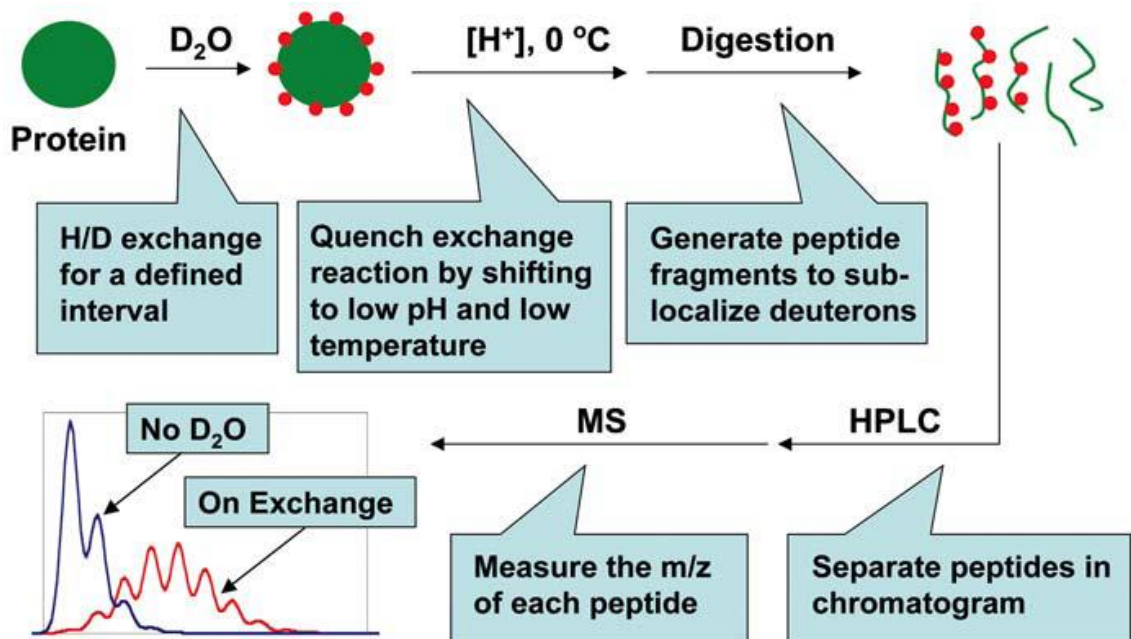Pure recombinant wt-TTR was used to run HX of backbone hydrogens with

Figure 16: HX coupled with proteolysis and MS overview. Extracted from ref. [27].

rapid and sensitive detection by MS. The protein was expressed and purified in-house while our collaborator Dr. Daniel Hirschberg (Helsinki University, Finland) carried out the HXMS experiments.

A stock of 100 µM TTR was diluted 50 times in a deuterated water PBS buffer (0,1 M NaCl, 3 M KCl, 10 mM Na_2HPO_4 and 2 mM KH_2PO_4 in D_2O) (Figure 16). 100-300 pmol aliquots of the sample were collected at different time points after the HX had been initiated. The hydrogen exchange-in was carried out at 4 and 22 °C for both the TTR samples and the different incubation times were 1, 18, 485 minutes and 1, 15, 60, 130, 500 minutes, respectively. Each aliquot was quenched by addition of 4 µL 2,5% (v/v) TFA per 100 µL aliquot to lower the pH to ~2,5. This step serves two purposes: first, to quench the exchange reaction and slow undesired back exchange to hydrogen; second, to mildly denature the analyte protein to facilitate digestion by pepsin. All subsequent procedures are conducted under the "quench conditions" to minimize the loss of incorporated deuterium [27]. The aliquot was snap-frozen in liquid nitrogen and stored until further analysis. Samples were thawed individually and loaded into a sample loop mounted on an injection valve (Figure 17). The deuterium incorporation was measured both on the intact and the pepsin digested protein (global and local HXMS, respectively). In global HXMS the mass increase of the intact TTR was followed over time while in local HXMS the protein was digested with pepsin prior to MS analysis, by changing the sample loop for a column with immobilized pepsin. The protein sample was digested for one minute on the pepsin column. Upon switching the valve to the inject position, the sample was flushed from the loop/pepsin column to a reverse phase Poros® 20 R2 microcolumn (Poros) where it was desalted with a flow of 400 µL/min 0.05 % (v/v) TFA. For global analysis, the sample was eluted directly from the trap column into the electrospray ion source with a flow of 80 % (v/v) acetonitrile and 0.05 % (v/v) TFA at 60 µl/min. For chromatographic separation of peptic peptides an analytical C4 column is mounted down-stream with the Poros® R2 microcolumn. Peptides were eluted with a 20-100 % (v/v) acetonitrile 9 min linear gradient, with a constant 0.05 % (v/v) concentration of TFA. For the MS analysis we used a quadrupole TOF electrospray ionization (ESI) (Q-ToF and Synapt G1, Waters) mass spectrometer. The peptic peptides yield information of regional HX kinetics. The HX rate is dependent on participation of hydrogen bonding, distance from protein surface, and flexibility of the

peptide chain. The retardation in exchange rate is heavily dependent on the protein structure and dynamics, and is termed the "protection factor" [27]. Sites where conformational changes have taken place, experience an increased/decreased protection factor in analyses of peptic digests of the labeled proteins [39]. The relative protection is determined against a fully deuterated sample determined by deuterium incubation at 65°C for 10 hours.

The local HXMS data was analyzed by HX-express [40]. Within this software one can see as a result a series of peptides found by the MS, where some of them overlap. This is wanted, since these peptides can be subtracted giving more resolution, i.e. ideally a single amide resolution. To calculate overlapping peptides that only differ
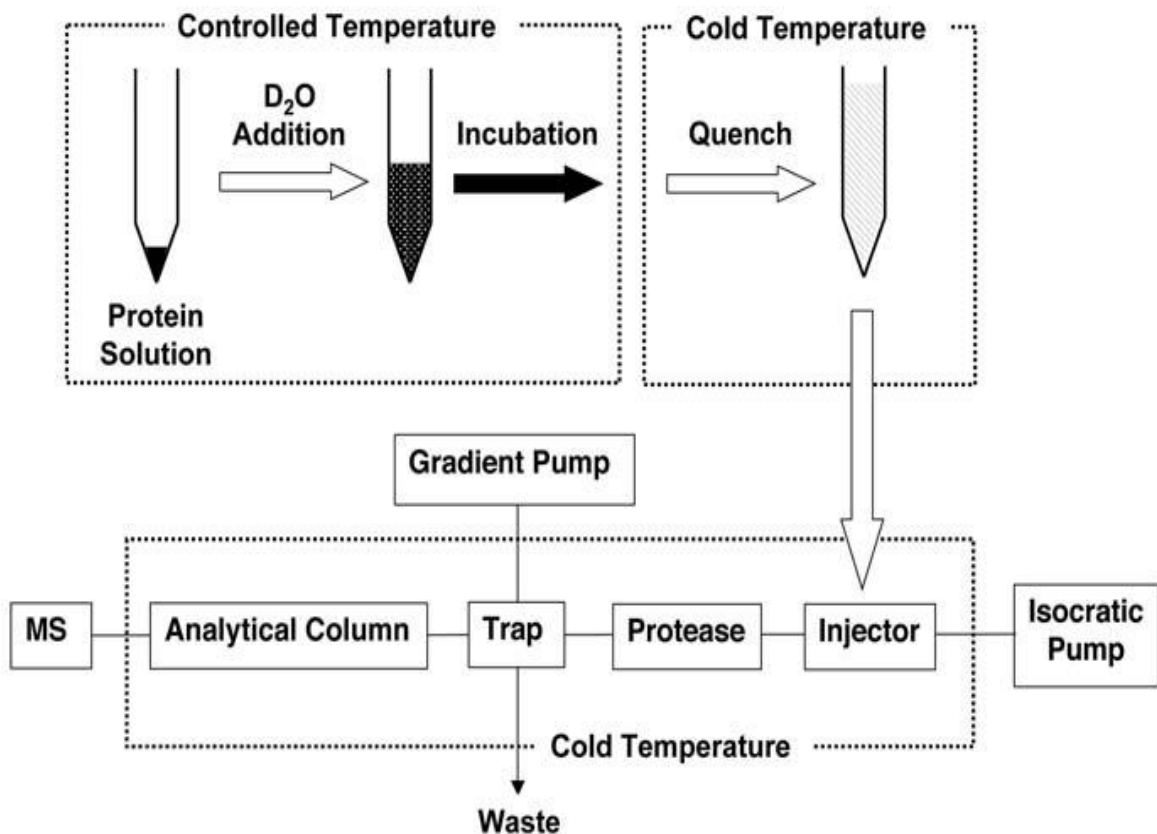
Figure 17: Automated flow diagram and temperature control. A liquid handler mixes the protein solution with the PBS deuterated buffer to initiate on-exchange, and adds the quench buffer after a defined incubation period. The quenched mixture is frozen and later thawed and introduced in the injector. Using an isocratic pump, the exchanged simple then flows from the injector through the protease column to a trap. After a valve switch, a gradient is used to elute peptides from the trap via the analytical column into the MS. Extracted from ref. [27].

in their C-terminal region the following formula was used [41]:

(D-content of region B-C) = (D-content of peptide A-C) - (D-content of peptide A-B)

*A, B and C being different amino acid positions in the sequence, where A<B<C.

To identify peptic peptides, non-deuteriated wt-TTR was digested and desalted as described above. The peptic peptides were then eluted and collected for LC-MS analysis. Data dependent acquisition is employed to obtain MS spectra of the peptic peptides. These spectra were searched by Mascot against a suitable database for peptide identification. The HXMS data for each time point was projected onto a crystal structure of the TTR complex using Pymol [42].

The back exchange varied from a few percent to 50% depending on the nature of the peptide and its elution time during local HXMS.

2.10.- NMR study using the two dimensional (2D) ^{15}N heteronuclear single quantum coherence (HSQC) experiment

In order to determine if conformational differences between RT and 4°C gel purified wt-TTR exist, a ^{15}N-^{1}H HSQC 2D experiment was carried out. In order to reduce dipolar relaxation arising from Cα bound protons, the protein sample was grown in the 99% deuterated medium as described in section 3.7, after which it was purified with regular protonated buffers as also mentioned previously. This triggered the isotope exchange from ^{2}H to ^{1}H of the labile amide groups of the polypeptide backbone, which was checked by MALDI and compared to a molecular weight prediction of the ^{15}N labeled partially deuterated sample and after all the labile positions are exchanged to ^{1}H [36, 43]. The degree of exchange was also tested in MALDI-TOF by previously

unfolding and refolding of the protein in order to exchange the protected positions and compare to the predicted one as well. This was done by a series of dialysis steps: against milliQ for protein desalting, in order to avoid aggregate formation through A-state [22]. The protein was then unfolded by pH 2 HCl solution to achieve a random coil (largely unstructured) conformation [22]. Then, it was refolded with the phosphate buffer used for gel filtration in order to increase the pH and therefore isotope exchange, which is at its minimum at pH 2,7 at room temperature [27].

Nonexchangeable Cα bound deuterons will stay in place even after the exchange, increasing sensitivity by avoiding transverse relaxation through dipolar coupling other than the one arising from amide ^{15}N-^{1}H couplings that were the subject of study [44].

We used a 600 MHz NMR spectrometer equipped with a triple resonance cryoprobe (Varian Inova). In order to determine if structural differences between wt-TTR purified at RT and 4°C exist, a ^{15}N-^{1}H HSQC was carried out. Wt-TTR from section 3.7 purified at RT was concentrated, finally giving a 225 µM wt-TTR, 90 mM NaCl, 45 mM Na-phosphate, 0,0045 g/L sodium azide, 10% D_2O, pH 7,5 protein sample. The 4°C protein was used at a concentration of 162 µM. The temperature of the sample probe was set at either RT or 4°C for the corresponding sample. The 2D spectrum of each sample was measured using a sensitivity enhanced ^{15}N-^{1}H transverse relaxation-optimized spectroscopy (TROSY) -HSQC, ideal for large proteins [45,46], and processed using the nmrPipe software to remove water peak, remove noise and Fourier transform the FID [19]. The 2D spectrum was analyzed using the SPARKY software [34].

3.- RESULTS

3.1.- Verification of protein integrity

3.1.1- SDS-PAGE followed by Coomassie staining

In order to confirm that the plasmid was successfully induced and to select correct fractions after IEC and gel filtration, SDS-PAGE followed by Coomassie staining was carried out. The samples collected before IPTG addition and just before harvesting cells were treated as described in materials and methods and the protein expression was confirmed. This was carried out for all protein preparations (during ^{15}N labeled and unlabeled protein production). Figure 18 A and B shows an example, in this case for the ^{15}N labeled sample. The OD_{660} before induction was 0,6 and raised to 1,2 at the moment of harvesting. It can be seen that a sharp band appears at a molecular weight of ~18 kDa.

In figure 18A, from well 5 to 10 we see IEC fractions 21-26 that were previously found to have a high absorbance peak at 280 nm at the end of the ionic strength gradient (data not shown). From these, fractions 22-25 were chosen to be purified by gel filtration.

In figure 18B, from well 1 to 8 we see the gel filtration fractions obtained at 4°C, 20-27, which just as after IEC, gave a peak of absorbance at 280 nm (data not shown). From these, fractions 21-25 were concentrated and submitted to confirmation by MALDI-TOF mass spectrometry.
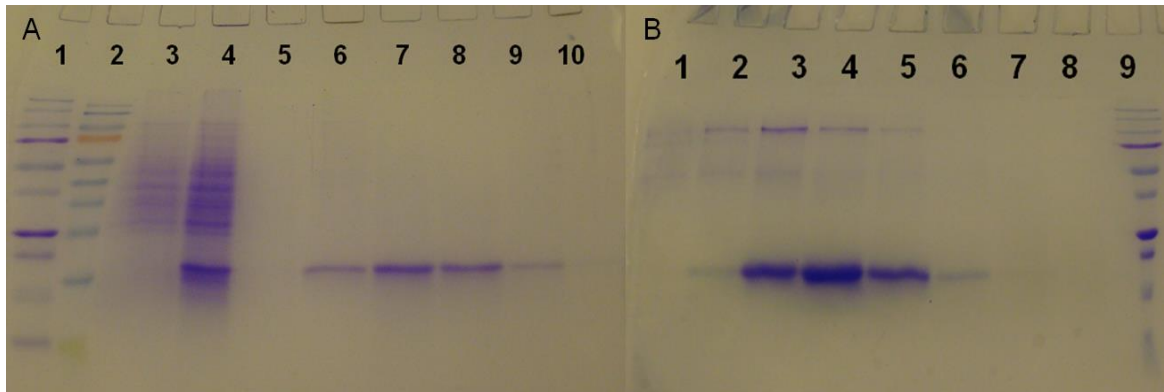
Figure 18: SDS-PAGE followed by Coomassie staining for confirmation of protein expression during bacterial culture and identification of desired protein fractions after IEC (A) and gel filtration (B). In gel **A**, **1:** 5 µL Precision Plus Protein™ Dual Color Standard (BIO-RAD) with different proteins of known molecular weight (250, 150, 100, 75, 50, 37, 25, 20, 15, 10); **2:** 5 µL PageRuler™ Prestained Protein Ladder (Fermentas Life Sciences) with different proteins with known molecular weights (170, 130, 95, 72, 55, 43, 34, 26, 17, 10); **3 and 4**: before and after plasmid induction by IPTG; **5 to 10:** IEC fractions 21 to 26. In gel B, **1 to 8:** gel filtration fractions 20 to 27; **9:** same protein standard as well number 1 in gel A.

3.1.2- Protein confirmation using MALDI-TOF mass spectrometry

With the objective of confirming the purity and integrity of different protein preparations, we performed MALDI-TOF mass spectrometry. A control spectrum with diluted protein buffer mixed with matrix solution can be seen in the following figure 19, which shows the appearance of a peak of low molecular weight.
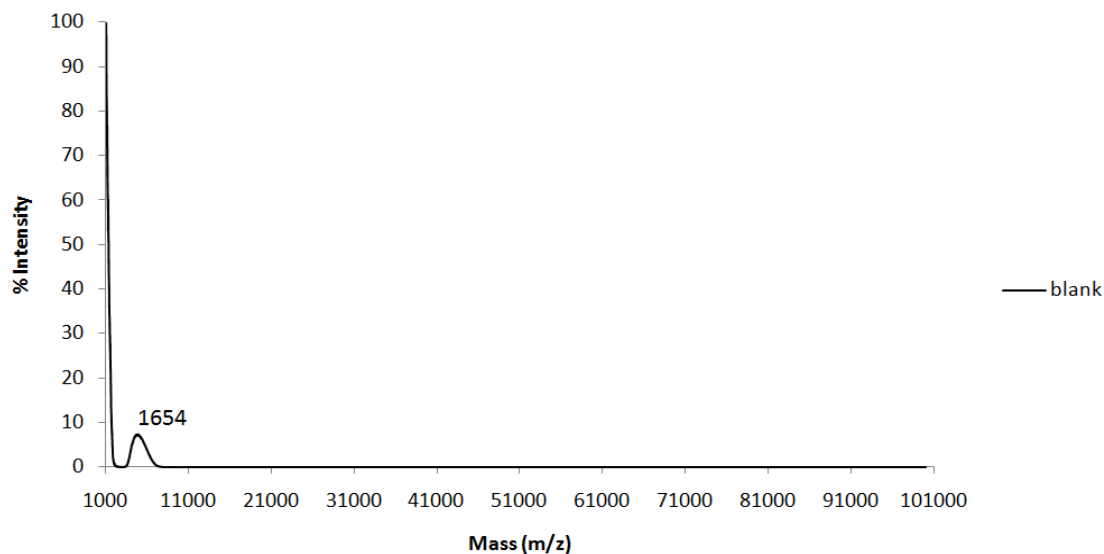
Figure 19: Control MALDI-TOF mass spectra. Spectra with a range from 1000 to 100000 m/z of a control solution of milliQ diluted phosphate buffer used for protein storage and sinapinic acid matrix solution. A sharp rise in signal <1000 m/z is due to background. The peak with the highest molecular weight appears at 1654 Da.

3.1.2.1- Unlabeled wt-TTR

In order to confirm the identity of the purified protein from section 2.5, we carried out a MALDI-TOF mass spectrometry analysis of the recombinant wt-TTR protein purified by IEC and gel filtration at either 4°C or RT (Figure 20). The molecular weight of 13893 Da for the 4°C purified TTR is perfectly in agreement with the theoretical molecular weight of 13892,6 Da for the recombinant wt-TTR protein (http://au.expasy.org/tools/protparam.html). In the case of RT purified recombinant wt-TTR, the weight has an absolute error of 0,05%, which is the maximum error for a 16953 kDa protein with external calibration [34]. Nevertheless, in this setup were not concerned about eliminating salts in the protein solution before the 40x dilution needed to achieve a final protein concentration of ~5 pmol/μL, which is in the range of the recommended concentration by the equipment provider. Buffers such as the phosphate

buffer used to store the protein sample can interfere with the molecular weight determination by increasing the number of sodium and potassium adducts in the
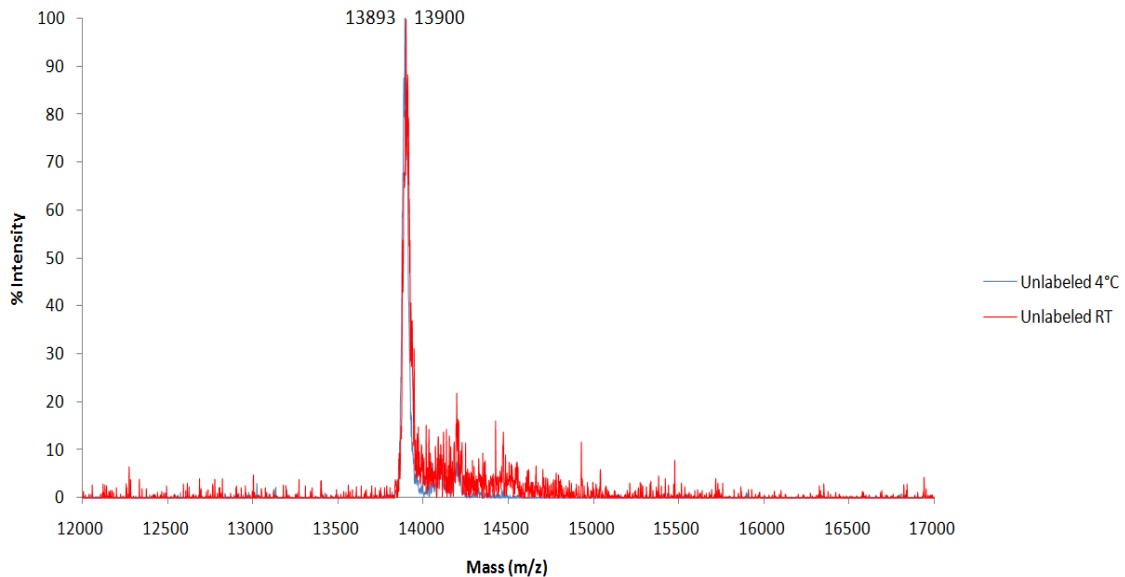
Figure 20: MALDI-TOF mass spectra of wt-TTR purified at RT or 4°C. Spectra with a range from 12000 to 17000 m/z of recombinant wt-TTR purified by gel filtration either at RT (red) or 4°C (blue). The peak for the 4°C and the RT samples were 13893 and 13900 Da, respectively.

spectra. This explains the small peaks on the right of the ~13900 wt-TTR peaks [34], as well as values up to 14000 Da in some of the MALDI-TOF checks for different preparations of the same protein. However, this approximation is good enough, along with the plasmid sequence translation (described in section 3.1) and SDS-PAGE, for determination of correct protein expression and purification, e.g. the plasmid expression was correctly induced, the right fractions were chosen and the protein was not digested by proteolysis.

3.1.2.2.- ^{15}N labeled wt-TTR grown in deuterated medium

In order to confirm the degree of isotope incorporation of the purified protein from section 3.7, we carried out a MALDI-TOF mass spectrometry analysis of the recombinant wt-TTR protein grown in 99% deuterated M9 medium with $^{15}NH_4Cl$ as the nitrogen isotope source and purified by IEC and gel filtration at either 4°C or RT (Figure 21). The maximum peaks were at 14675 and 14717 Da, respectively. The estimated molecular weight for recombinant wt-TTR with 100% ^{15}N and partial ^{2}H labeling is 14866 Da. After all labile positions are exchanged to ^{1}H, the molecular weight is estimated to be 14685 Da [43]. Analyzing both peaks, it is evident that the 4°C compared to the RT sample has a narrower distribution and that both peaks are broader than those peaks for unlabeled TTR. At 50% intensity the width of each peak is 100, 311 and 37 Da for the labeled 4°C, RT and unlabeled 4°C protein samples, respectively (unlabeled 4°C protein was chosen for this comparison because it had higher signal to noise ratio).
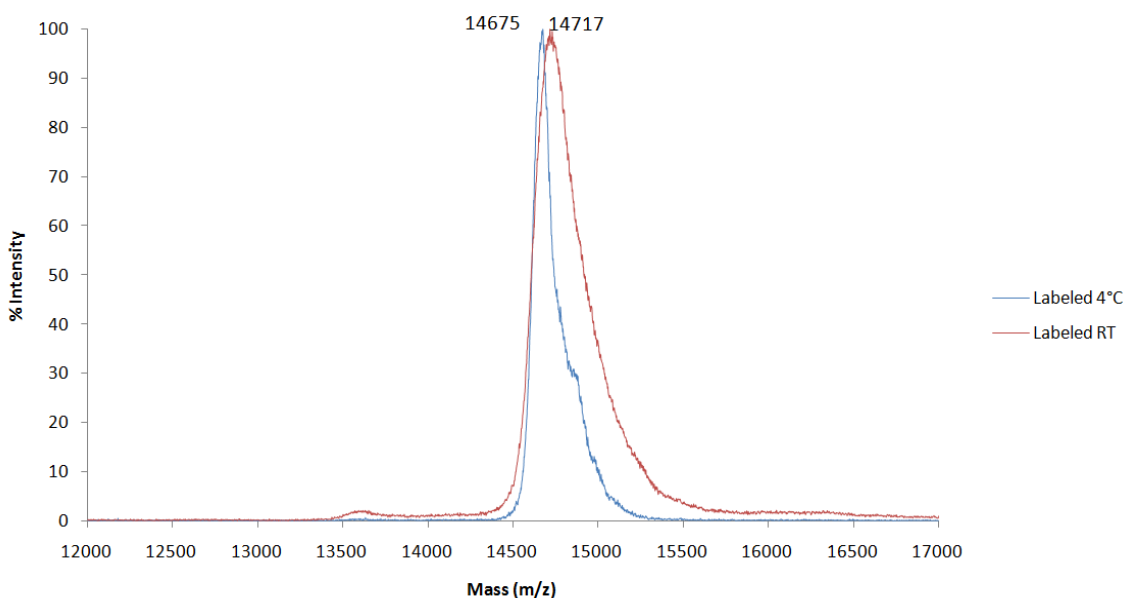
Figure 21: MALDI-TOF mass spectra of ^{15}N labeled wt-TTR purified at RT or 4°C. Spectra with a range from 12000 to 17000 m/z of ^{15}N labeled recombinant wt-TTR purified and stored either at RT (red) or 4°C (blue). Peaks for the 4°C and RT samples were 14675 and 14717 Da, respectively.

3.1.2.3- ¹⁵N labeled wt-TTR grown in deuterated medium, after isotope exchange

In order to confirm the degree of isotope exchange that the ^{15}N labeled samples grown in 99% deuterated M9 medium underwent throughout the purification protocol, we carried out a MALDI-TOF mass spectrometry analysis of both samples after dialysis against milliQ for 1 day, two days of dialysis against pH 2 HCl medium and 1 day of refolding by dialysis in phosphate buffer pH 7,5 (Figure 22). This allowed proton exchange in the positions where the solvent was inaccessible during the purification protocol. The maximum peaks were at 14719 and 14757 Da, for 4°C and RT proteins, respectively. The estimated molecular weight when all the positions are exchanged to ^{1}H is 14685 Da [43]. The width of the peaks at 50% intensity is exactly 188 for both samples.

The ~60 Da absolute error between the expected value might be explained by
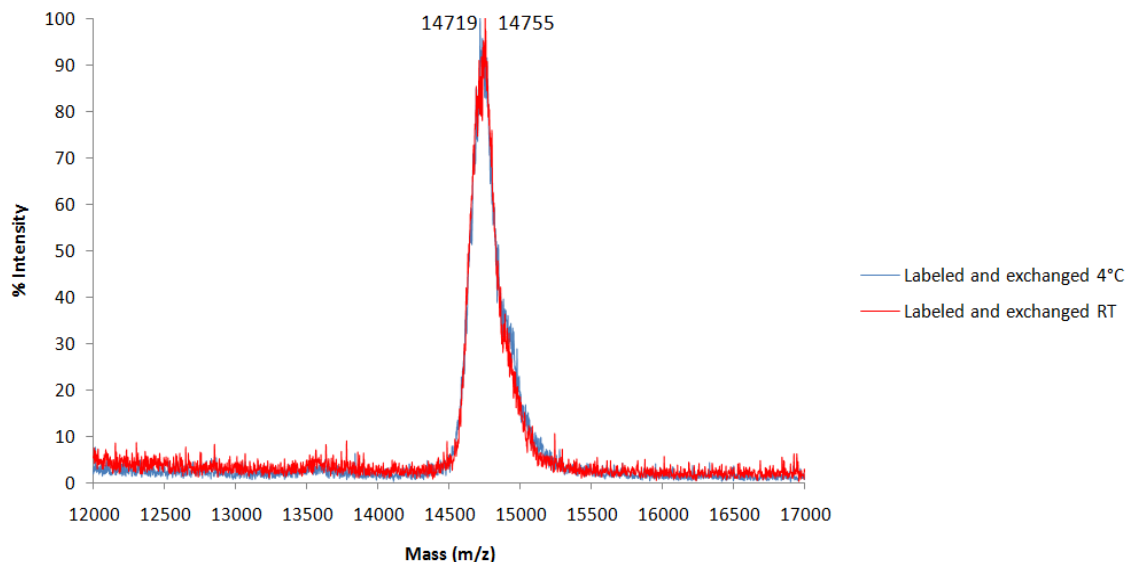

Figure 22: MALDI-TOF mass spectra of ^{15}N labeled wt-TTR purified at RT or 4°C, after isotope exchange. Spectra with a range from 12000 to 17000 m/z of ^{15}N labeled recombinant wt-TTR purified by gel filtration either at RT (red) or 4°C (blue). Peaks for the 4°C and RT samples were 14719 and 14755 Da, respectively.

the high sodium content of the protein samples, because they were not diluted before the analysis. However, this is enough to depict the difference in degree of exchange for the protein samples, after the purification protocol, which is shown as an overlay of the previous spectra in figure 23.
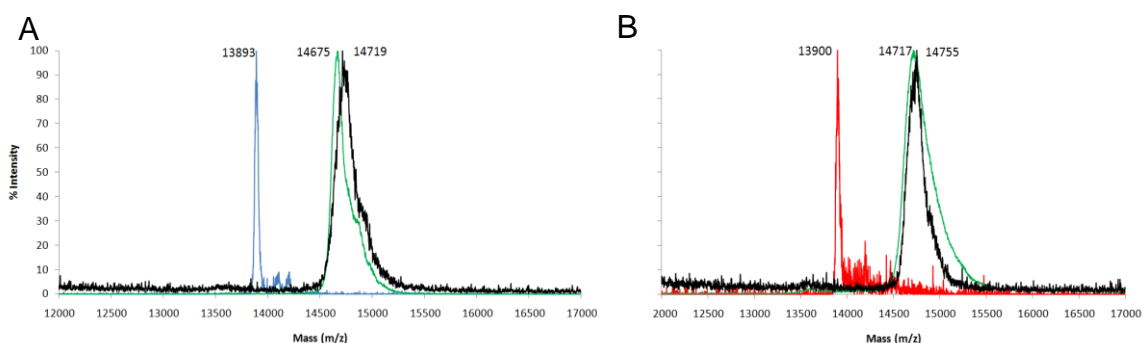
Figure 23: Overlay of MALDI-TOF mass spectra of unlabeled, ^{15}N labeled and after isotope exchange of wt-TTR purified at RT or 4°C. Spectra with a range from 12000 to 17000 m/z of recombinant wt-TTR purified by gel filtration either at 4°C (A) or RT (B), showing the increase in molecular weight upon ^{15}N labeling of the protein in deuterated M9 medium (green), which then was submitted to full exchange by unfolding and refolding (black).

3.1.2.4 - Formation of TTR multimers during MALDI-TOF analysis

A phenomenon of unknown relevance was observed during the previous analyses, consisting of the appearance of high molecular weight non physiological multimers of the protein under study both for the labeled and the unlabeled proteins, as can be seen in figure 24. The number of multimer peaks that could be seen was up to hexamers and the monomer to multimer intensity ratio varied from measurement to measurement for reasons that can not currently be identified. The appearance of these multimers could neither be modified by submitting the protein samples to dialysis against pH 2 solution with HCl (random coil induction) nor by stabilizing 4,15 µM

43

tetramer by incubating with 10 µM of the T_4 analog, diflunisal (data not shown), which has a K_{d1} of 75 nM and a K_{d2} of 1,1 µM for 1,8 µM tetramer [48].
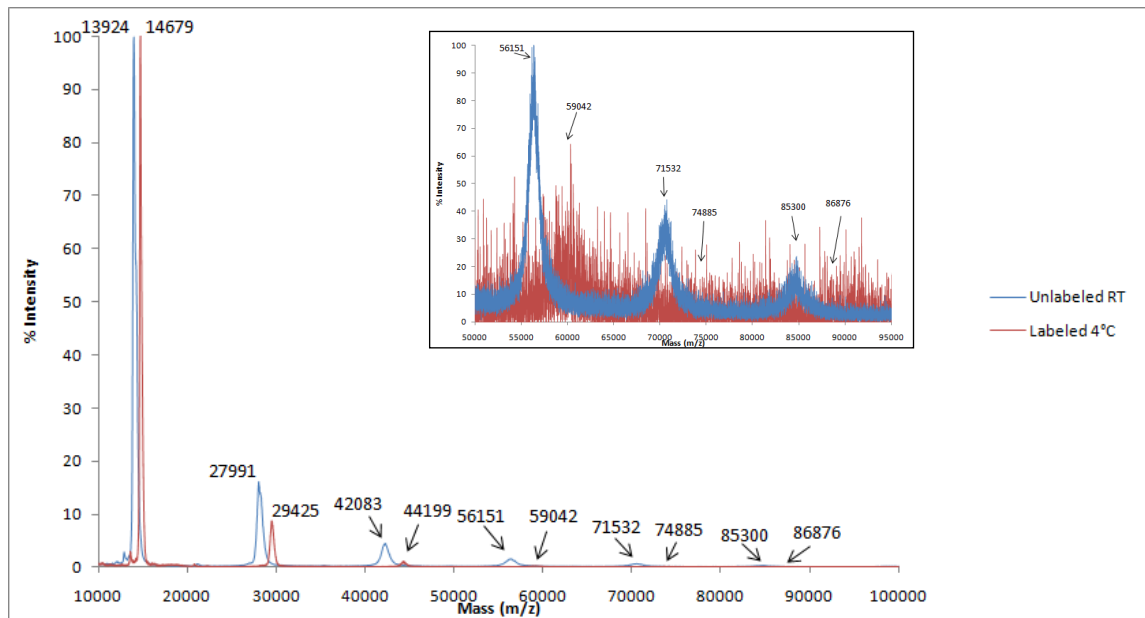
Figure 24: Overlay of MALDI-TOF mass spectra of unlabeled wt-TTR gel filtered at RT and ^{15}N labeled wt-TTR at 4°C showing multimers formed during analysis. Spectra with a range from 10000 to 100000 m/z of unlabeled recombinant wt-TTR gel filtered at RT (blue) and ^{15}N labeled at 4°C. Up to 6 monomers containing multimers are shown. The insert shows the same spectra with percent intensity relative to the most intense peak, with a range from 50000 to 95000 m/z.

3.2.- Tetramer dissociation kinetics

The rate of quaternary structural changes can be detected by linking tetramer dissociation to TTR tertiary structure unfolding. This is due to the rapid monomer unfolding, which is five to six orders of magnitude faster than tetrameric TTR dissociation, and therefore the rate-determining dissociation step was measured by linking the quaternary structural changes to tertiary structural changes (measured by

tryptophan fluorescence) mediated by 6 M urea [38]. Using urea concentrations in the post-transition region for tertiary structural changes directly links the slow TTR quaternary structural changes to the rapid tertiary structural changes and renders unfolding irreversible [23].

Dissociation time courses for wt-TTR purified at RT and at 4°C in 6,0 M urea are shown in figure 25A. The kinetics fits well to a single exponential function (R^2 are 0,99 and 1,00, respectively).

The urea unfolding rate for wt-TTR purified at RT was slower, as expected, with a dissociation rate ($t_{1/2}$) of 19,1 hours compared to 7,4 hours for the 4°C purified protein, the latter therefore dissociating 2,6 fold faster. Tetramer dissociation rates (k_{diss}) were 0,36 h^{-1} and 0,94 h^{-1}, respectively.
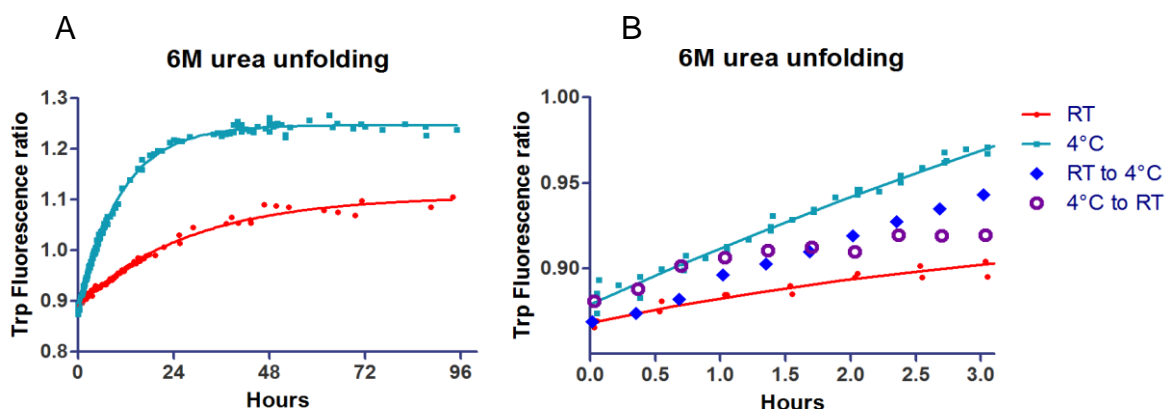
Figure 25: Urea unfolding curves of wt-TTR at different temperatures.   The tryptophan fluorescence ratio and the fittings were performed as described in materials and methods. A) Kinetics of 6,0 M urea unfolding for RT and 4°C protein. B) Close-up view of the temperature jump experiment.

The fluorescence intensity maxima for 4°C wt-TTR was 2000 at 340 nm and decreased to 990 at 349 nm after 92 hours, when for RT wt-TTR was 1500 at 340 nm and decreased to 973 at 347 nm after 92 hours.

The temperature jump experiment was carried out also at 6,0 M urea (Figure 25B).   The concentrated samples in phosphate buffer at their corresponding temperatures were quickly ~50 fold diluted into a pre-equilibrated urea buffer at the opposite temperature before starting fluorescence measurement. The unfolding curves displayed an inflection point at around 30-60 minutes after the beginning of the

experiment and thereafter followed the fluorescence emission denaturing behavior corresponding to their final temperature. The temperature jump curves never collided with the original fits during the first 20 hours of fluorescence measurement (data not shown).

3.3.- HXMS

An HXMS exchange-in study was carried out in order to find differences in terms of ^{2}H incorporation by incubation of 4°C and RT purified wt-TTR samples in deuterated PBS buffer at either 4°C or 22°C. No difference was found in terms of exchange pattern after global exchange was carried out at RT for both TTR samples (data not shown). However, local HXMS was run to search for at least small differences among peptic peptides, which give an idea of regional HX kinetics [27]. It was not necessary to perform a MS characterization of peptic peptides because the peptic cleavage was similar to a previous one performed with the same protein.

At RT, the peptic peptides analyzed covered the whole protein sequence and gave no clear differences among the two protein samples in terms of deuterium incorporation in the 1, 15, 60, 130, 500 minutes intervals analyzed (Figure 26). In the HXMS experiment carried out at 4°C, no significant differences were found either by incubating at 1, 18, 485 minutes (Figure 27).

Next, the HXMS data for each time point was projected onto a crystal structure of the TTR monomer to show the heat map of deuterium incorporation (Figure 28). In these heat maps, the 4°C purified wt-TTR sample results obtained at 4°C are compared with RT purified wt-TTR sample results obtained at 22°C. One can see that as expected, at 4°C the overall exchange is lower from slower chemical exchange at lower temperature. It can also be seen that the N-terminal region of the 4°C sample shows higher isotope incorporation compared to the RT sample, comparing both after 1 minute incubation; in detail, they exhibit 83,07 and 79,66% of deuterium incorporation, respectively. This higher degree of incorporation is still observable when comparing
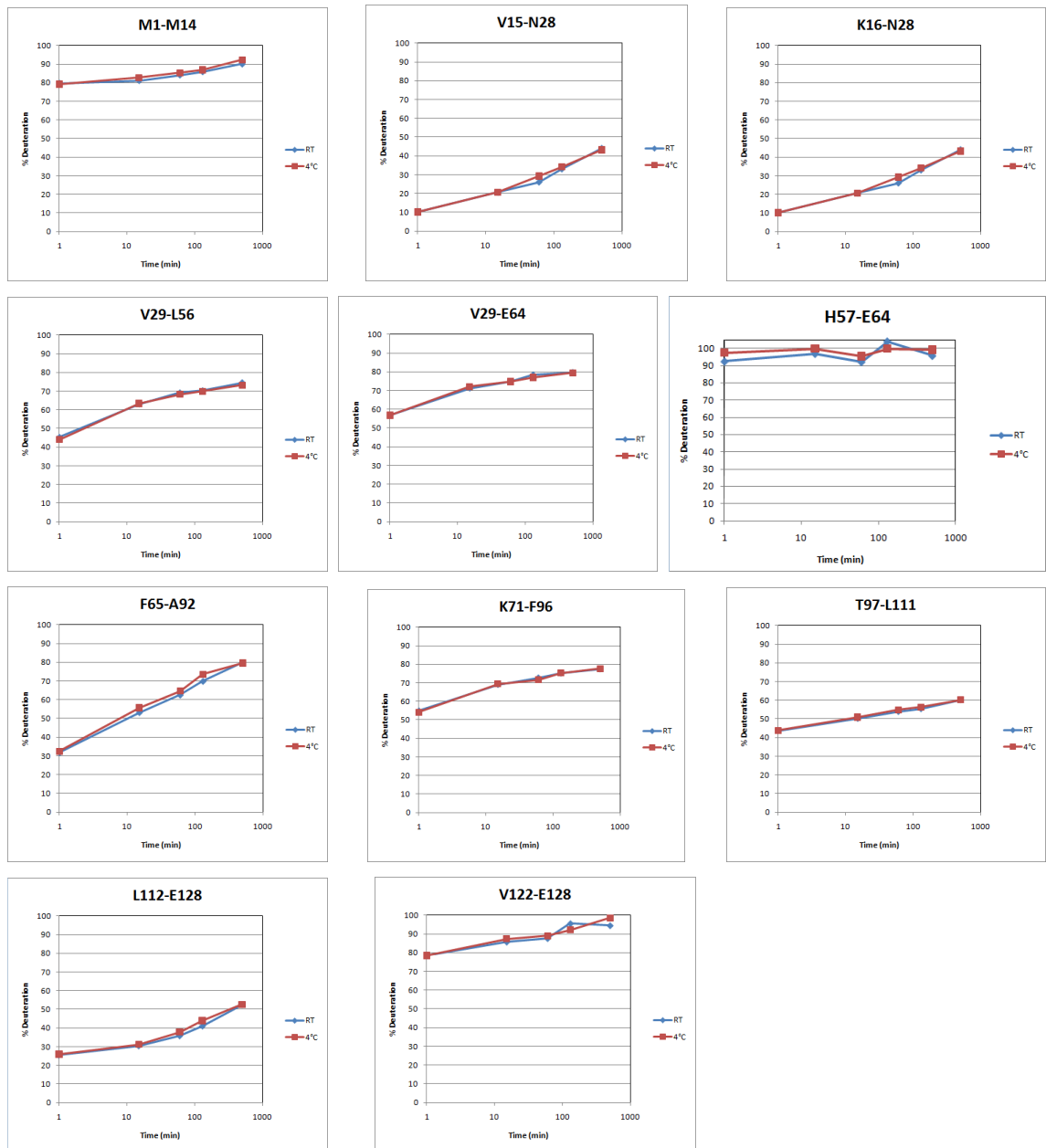
Figure 26: Deuterium uptake at 22°C of wt-TTR purified either at RT (blue) or 4°C (red) at 1, 15, 60, 130 and 500 minutes intervals. H57-E64 peptic peptide was calculated using a simple subtraction of deuterium contents in peptides V29-L56 and V29-E64, as described in materials and methods.
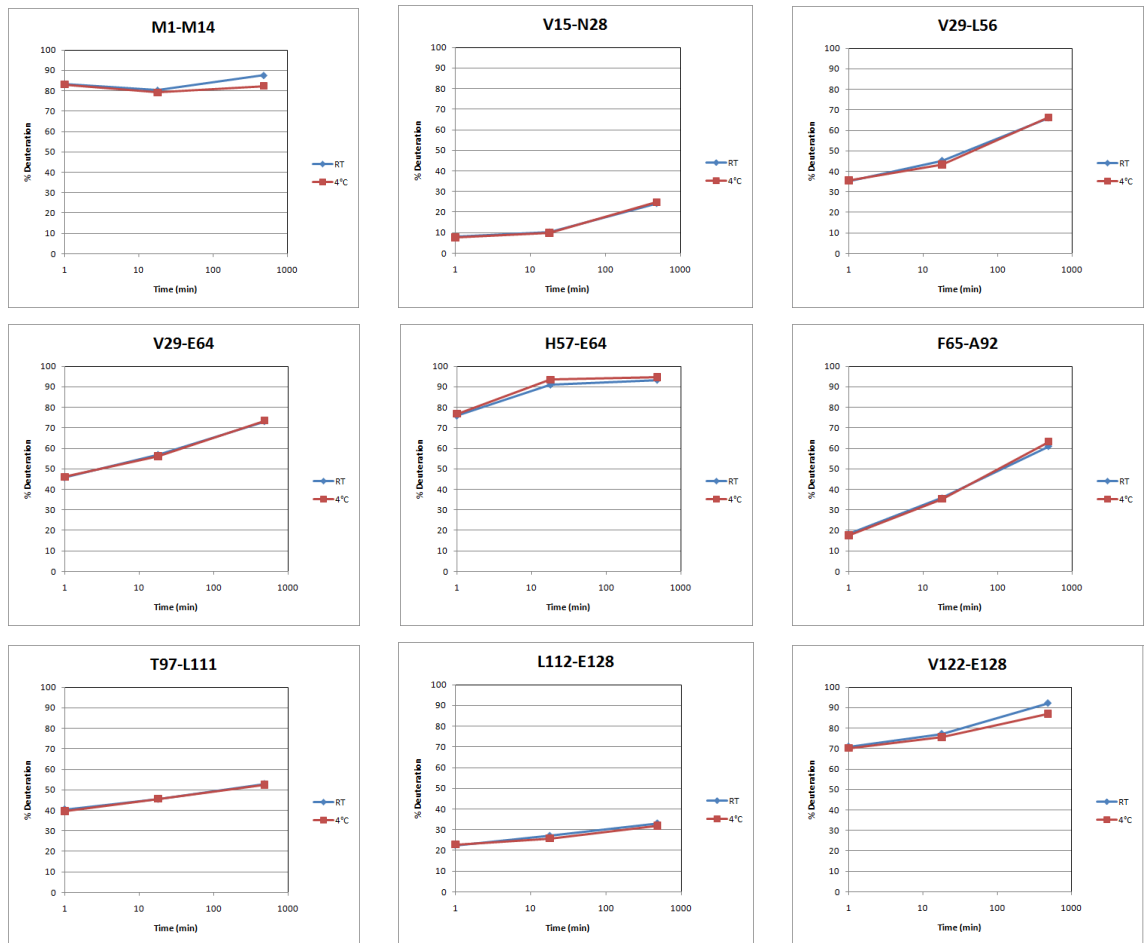
Figure 27: Deuterium uptake at 4°C of wt-TTR purified either at RT (blue) of 4°C (red) at 1, 18 and 485 minutes intervals. L56-E64 peptic peptide was calculated using a simple subtraction of deuterium contents in peptides V29-L56 and V29-E64, as described in materials and methods.
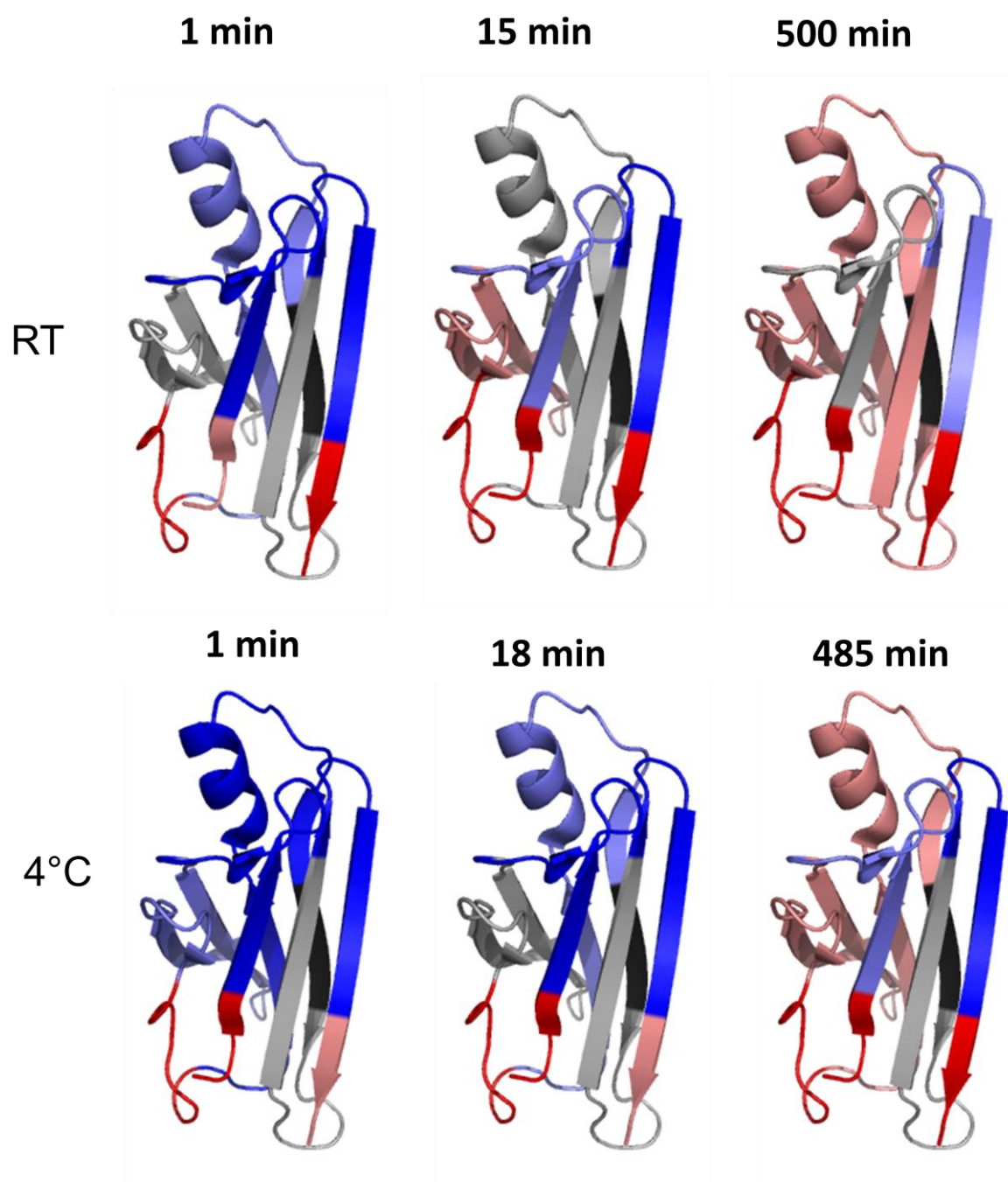
Figure 28: Ribbon diagram representation of local deuterium uptake of wt-TTR purified at RT in the HXMS run performed at 22°C, side-to-side with the 4°C purified protein in the experiment carried out at 4°C. Color codes that represent different percents of deuterium exchange are as follows:
Blue 0-20%; **Light blue** 20-40%; **Grey** 40-60%; **Light red** 60-80%; **Red** 80-100%.

with the RT sample that has exchanged for 15 minutes. The observation is more remarkable if we consider that the rate of isotope incorporation should be higher at 22°C compared to 4°C; comparing these samples at the same time points can be misleading, since different chemical exchange must be compensated, so only differences in deuterium incorporation due to possible differences in structure are compared. Therefore, in order to get closer to a real comparison, we can consider the 7 fold higher intrinsic exchange rate at 22°C compared to 4°C, which is estimated in the base of the isotope exchange rate of a linear peptide using Sphere software available in the http://www.fccc.edu/research/labs/roder/sphere/sphere_help.html website [49, 50]. The rate of subunit exchange of TTR is 3 fold faster at 4°C compared to 37°C and therefore would be about 1,6 fold faster if compared to 22°C [25], assuming the rate changes linearly with temperature. Having stated these assumptions, we can roughly compare the 1 minute time point of figure 28 – RT with the 4°C 18 minute one and the 15 minute RT with the 485 minute 4°C one; by this approximation we have overcompensated 18 times and 32 times, respectively, for the slower intrinsic exchange at 4°C, by using a longer incubation time for the slower exchanging 4°C run. One can say then that we have compensated the difference in intrinsic exchange rate by 2,6 and 4,6 fold, respectively. The faster subunit exchange should add to this compensation factor of 1,6.   Hence the comparisons overcompensate 4,2 and 7,36 times, respectively, for the slower exchange rate at 4°C. According to these analyses, it would be significant if we find peptic peptides that have a lower incorporation at 4°C using these time points.

Then, we found also that a crucial peptide, which contains the b-c loop, V29-L56, is slightly protected at 4°C at the 18 minutes time point compared to the 1 minute time point at RT, with 43,36 and 45,28% of deuterium incorporation, respectively. This same higher protection was found analyzing the same pair of time points for the peptide V29-E64 that interestingly also covers the b-c loop, with 56,12 and 56,63% protection, respectively. Again, comparing the same respective time points we also found that the V15-N28 peptic peptide has a higher degree of protection, with 9,17 and 10,16%, respectively.   Also, the C-terminal V122-E128 peptide also has a lower degree of incorporation at 4°C, with 75,64 and 78,47%, respectively. The peptide generated by subtraction of peptides V29-E64 and V29-L56, H57-E64, gave lower protection for

these time points (90,96 and 92,46) and also comparing the 485 minutes for 4°C and the 15 minutes time points, with 93,26 and 96,89%, respectively.

3.4.- ^{15}N-^{1}H HSQC

With the aim to determine at an atomic level resolution whether structural differences arose from the temperature difference at which wt-TTR was purified and stored, a J-coupling ^{15}N-^{1}H HSQC experiment was carried out at either 4°C for the 4°C purified protein or 22°C for the RT purified one, and the following 2D spectra were obtained (Figure 29). As expected, due to the lower temperature and lower concentration of the protein sample at 4°C, only 79% of the peaks in RT were found by visual inspection. Rotational correlation time is expected to increase as temperature drops, due to slower molecular tumbling. This temperature effect decreases the averaging of dipole-dipole interactions, in the same fashion as a larger protein increases line broadening [30]. In this case, native tetrameric wt-TTR has a molecular weight of ~56kDa, which was considered too high to allow sensitive NMR measurements [51]. However, recently a 82kDa protein whole 3D structure has been determined with a combination of techniques [28]. The concentration typically required for an NMR experiment is 1 mM, although spectra using as low as 50 µM protein have been obtained [31]. However, the 1,6 fold increased subunit exchange from 22°C to 4°C, commented in the previous chapter, compensated to the slow tumbling hence increasing sensitivity.

The number of peaks manually identified at 22°C was 149 out of a theoretical maximum of 145 if all the ^{15}N-^{1}H couplings in the protein give rise to a peak. This indicates that probably all the labile position were exchanged by protons during the purification process, which is also supported by the non decrease in molecular weight during unfolding and refolding checked by MALDI-TOF (figure 23). It was not possible to use the backbone assignment previously published [23], where 120 non proline
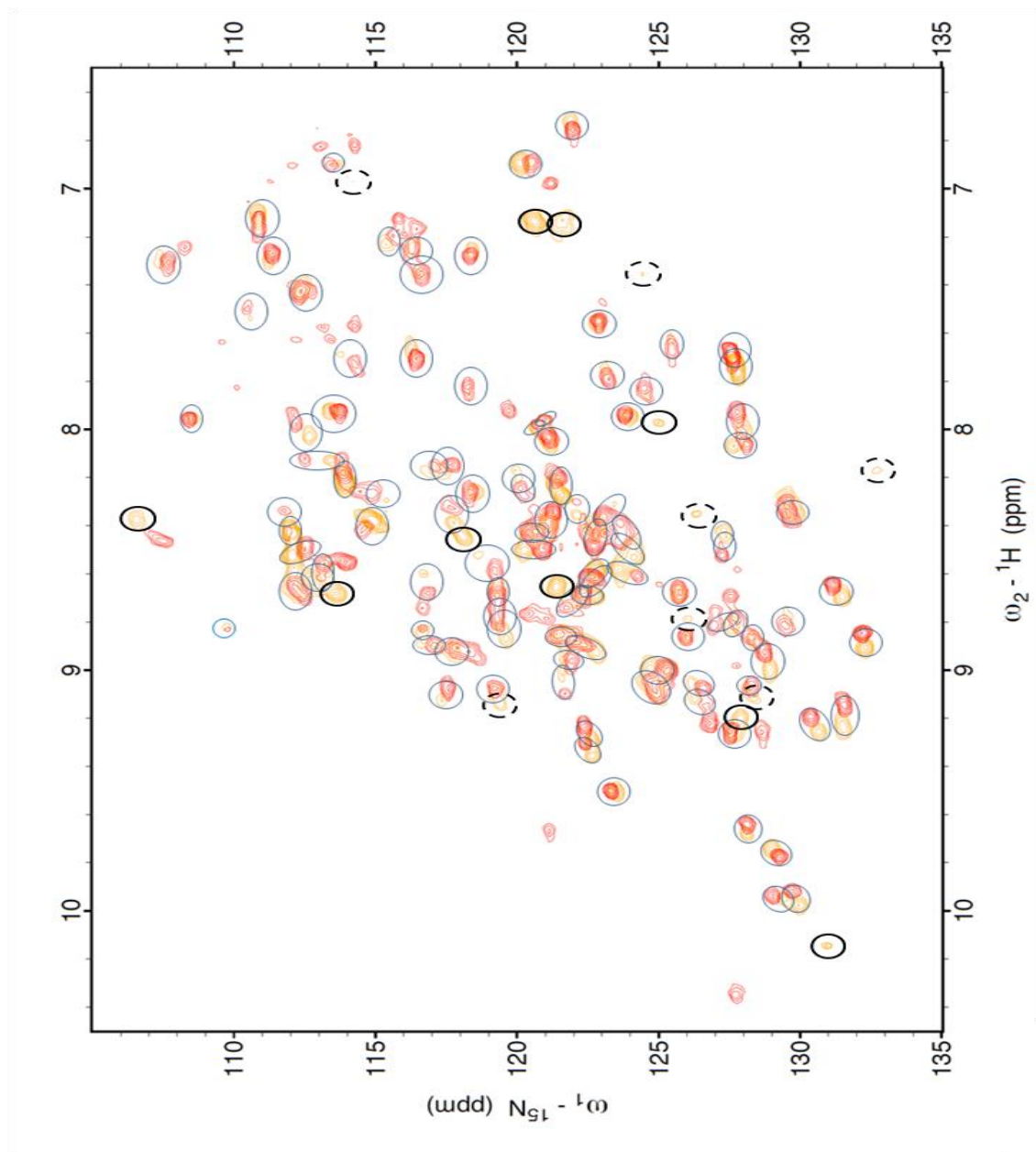
Figure 29: Overlay of ^{15}N-^{1}H HSQC spectra of wt-TTR at 22°C and 4°C. Wt-TTR at 22°C (red) or 4°C (yellow), were purified also at these temperatures. Selected are the overlaying peaks which were manually identified to be separated by at most 0,1 ppm of chemical shift in the ^{1}H dimension of 0,2 in the ^{15}N dimension (blue circles). The total number of peaks determined manually at 22°C and 4°C was 149 and 117, respectively, while 101 fell in the overlaying criteria stated above. 9 peaks out of 16 obtained at 4°C displayed high intensity and could not be matched with peaks obtained at RT (black circles). 7 peaks out of 16 obtained at 4°C displayed low intensity and could not be matched with peaks obtained at RT (dashed black circles).

backbone residues were assigned, because most of the peaks were in different positions (data not shown), probably due to the different pH and temperature, which were 5,75 and 30°C, in their study. Therefore, in order to compare the amount of overlaying peaks of both spectra, we compared the number of peaks at 4°C that could be matched with a peak from the spectrum at 22°C within a 0,1 ppm chemical shift difference in the ^{1}H dimension and 0,2 ppm chemical shift in the ^{15}N dimension. Using these criteria, 16 out of 117 peaks in the 4°C 2D spectra were not possible to match with any of the 22°C spectra. Among these, the 9 displayed high intensity (Table 3). High intensity peaks are more reliable since at 4°C sensitivity is lower, decreasing signal:noise ratio.

Table 3: Selection of intense peaks in the ^{15}N-^{1}H HSQC spectra.									
Nuclei	Chemical Shift (ppm)								
^{1}H	7,15	7,15	7,88	8,4	8,42	8,61	8,65	9,2	10,15
^{15}N	120,5	121,5	125	106,5	118	121,5	114	125,6	131

4.- DISCUSSION

The earlier observation by our laboratory that cold purified and stored native tetrameric wt-TTR at 4°C is cytotoxic in cell culture, with similar toxicity to the most toxic aggregates [13] opened our eyes to look closer in understanding this molecule and its structure. We are interested in determining what exactly makes tetrameric wt-TTR at 4°C more toxic than the tetrameric wt-TTR purified and stored at RT. Unpublished experiments using small angle X-ray scattering, circular dichroism and tryptophan fluorescence have indicated that a slight conformational change is likely to happen, although little is known about where this conformational change is taking place in the molecule. What is known is that at 4°C the protein is less resistant, compared to 25 and 37°C, towards urea induced denaturation. TTR tetramers do not denature in urea; hence, dissociation to monomers is required for urea induced tertiary structural changes to be detected by tryptophan fluorescence [38]. Faster cold tetramer dissociation likely happens because of destabilization of the hydrophobic core of the protein, the main stabilizer of the structure, due to a decrease in the hydrophobic effect at lower temperature, facilitating cold denaturation [26, 52]. This also, as elegantly determined by subunit exchange experiments using ion exchange chromatography to separate a mixture of native and charge modified tetramers as a function of time and temperature, explains why the rate of subunit exchange is 3 fold faster at 4°C compared to 37°C [25]. One more clue into possible conformational changes in TTR structure due to lower temperature is a decrease in solvent accessibility to the loop between the strands c and b. This could be determined from the lower quenching experienced at 4°C during fluorescence measurements and is in agreement with acrylamide quenching of Trp-41 residue [13]. This residue is responsible mainly for TTR's fluorescence emission spectra, since Trp-79 is largely quenched in native TTR's structure [22].

Herein, we carried out a series of experiments in order to find structural differences between 4°C and 22°C in the tetrameric structure of TTR. X-ray crystallographic studies are unsuitable to use in these cases, since TTR mutants that

are highly amyloidogenic reveal native-like tertiary structure, providing little insight into small conformational changes [19].

Our strategy included wt-TTR expression in BL21/DE3 *E. coli* strain and purification by IEC and gel filtration chromatography. The former procedure was always performed in a cold (4°C room) and the latter carried out either at 4°C or RT (22°C), as previously described [13]. It was not possible to determine why purified TTR migrated slower than expected in SDS-PAGE, giving an average molecular weight of ~18 kDa for the protein that was ^{15}N labeled (figure 18) and ~16 for the unlabeled protein (data not shown). However, the sequence to be expressed was confirmed and the molecular weight of the protein was always checked by MALDI-TOF, giving a range from about 13900 to 14000 Da of molecular weight for the unlabeled protein, for about 6 different preparations (data not shown). Also, a control experiment using pure lysozyme (14,6 kDa) as a reference protein showed normal migration, running next to a 15 kDa molecular weight standard (data not shown).

Slight variations during MALDI-TOF molecular weight determinations can be attributed to salts in the protein stock solutions, because these were stored at different concentrations, ranging from 1 to 5 mg/mL in the case of the unlabeled protein preparations. Protein solutions should ideally be desalted before MALDI-TOF measurements, because phosphate buffers can interfere with accurate measurements [34]. However, these slight differences of about 100 Da do not interfere in the determination of correct protein expression and purification of unlabeled samples (figure 20) or ^{15}N labeled wt-TTR grown in deuterated medium. The latter showed an interesting peak broadening compared to the unlabeled wt-TTR peak, which is most likely due to the 99% D_2O growth medium, which would make the bacteria generate proteins with a Gaussian distribution of molecular weights due to a slight randomness in the water intake that would actually favor protonated water use due to its higher efficiency to promote bacterial metabolism compared to deuterated water [53]. It was very interesting to see that, as expected from the faster subunit exchange, the labeled sample that was gel filtered at 4°C showed a smaller weight (14675 Da) compared to the RT (14717 Da). This indicates that exchange-out of the deuterons in the protein was more favored, which is possibly responsible for the wider distribution of molecular weights towards higher molecular weights for the RT gel filtered sample (figure 21).

This difference in peak broadening was nicely evened by unfolding and refolding at pH 7,5, although the molecular weight increased in both cases (figure 22), probably because these refolded samples were not diluted and mixed directly with matrix solution, therefore leaving undesired phosphate buffer in the sample solution.

Herein we report the formation of multimer ions of TTR during MALDI-TOF mass spectrometry analyses for both labeled and unlabeled samples (Figure 24). During this type of analysis, routinely only single and double charged protein molecular ions are observed, which facilitates the spectral interpretation. Peaks composed for up to 6 monomeric subunits were identified over noise level. This phenomenon is likely happening due to random association after the proteins have been vaporized into the gas phase through the assistance of the laser and matrix and have been reported only once in the literature by Lee et al. [54]. Interestingly, they found that proteins that are not related have a lower tendency to form multimers; however, the importance of this random association for TTR related studies is unknown.

The effect of temperature on TTR stability was assessed at 4°C and RT in order to corroborate the behavior, shown in a previous publication [26], towards denaturation using chaotropic agents such as urea, which lower protein stability proportional to their concentration. Urea is thought to interact preferentially with the hydrophobic groups in the denatured state; however, the binding is very weak, which may explain the high concentrations required [55]. TTR exhibited a red shift and a quenching (decrease in emission intensity) in the spectra, likely due to the exposure to solvent and subsequent quenching of trp-41 mainly, since trp-79 is intrinsically quenched and when de-quenched due to denaturation it only slightly increases emission intensity [22]. From the higher intensity maxima at 4°C compared to RT we can extract that trp-41 is likely to be more buried in the molecule, which would explain the lesser quenching experienced. We can also extract from the incomplete red shift experienced at RT after 92 hours that the protein at this temperature doesn't experience the same degree of unfolding. This is also supported by the lower fluorescence emission 355/335 nm ratio and the previous study where at 37°C the protein could not be completely unfolded by urea. Wt-TTR at 4°C proved to be 2,6 fold faster than at RT, comparing each k_{diss}. Since the hydrophobic effect is weaker at lower temperature, this corroborates that hydrophobic interactions play a major role in stabilizing TTR tetramer [26]. This decreased stability

is also corroborated by pressure induced denaturation studies where TTR was less stable at 4°C compared to 37°C, also increasing the concentration of the monomer fraction 3 times [56], and by the above mentioned faster subunit exchange when the temperature is decreased [25]. From the temperature jump experiment (Figure 25B) it is tempting to hypothesize that a conformational transition from 4°C to RT and vice-versa is happening between 30 and 60 minutes after the beginning of unfolding, although it can't be ruled out that the unfolding itself could be accelerating this transition. A future temperature jump using NMR spectroscopy could solve the problem in a more physiological chemical environment in order to have an idea of when this conformational change occurs and. This would be useful for practical laboratory experimental purposes and to define whether when a patient is receiving wt-TTR that once was submitted to cold storing, i.e. a liver transplant or blood transfusion, is also receiving toxic TTR species.

The HXMS results should be analyzed cautiously, since after the experiment we found out that to experimentally measure a fully deuterated peptide, denaturation at 65°C for several hours was used, but TTR doesn't commence unfolding at <80°C [26]. However, it can be used as a guide for sites to keep an eye on in following studies, as possible sites of increased/decreased protection. It is feasible that the conformational change occurs before the first time point (1 minute), which would explain why no evident changes are observed. Nevertheless, comparing each sample in the run carried out at their corresponding temperature makes likely that a less restrained N-terminal segment is happening at 4°C. Differences found using stretchy comparisons such as that the c-b loop is more conformationally restrained, as well as the V15-N28 segment and the C-terminal region, should also be interpreted cautiously. A new HXMS experiment is required, this time taking in consideration the high thermal stability of TTR, hence measuring the fully deuterated peptides using deuterated urea medium in order to unfold and fully deuterate the protein before running local HXMS. This would give further clues into which fragments of the molecule become more or less protected to solvent due to the temperature drop.

The 2D spectra obtained by NMR spectroscopy confirmed that minor structural differences exist among the two samples. Although sensitivity as expected was lower at 4°C because of slower molecular tumbling and lower protein concentration compared

to RT, the high in concentration likely increased the 1,6 fold faster rate of subunit exchange from 4 to 22°C by a factor of 2,9 and therefore a total of 4,6 fold compared to RT, assuming that the rate of subunit exchange changes linearly from 4°C to 37°C, which were the rates experimentally determined previously [25]. This increased the sensitivity allowing us to identify clear ^{15}N-^{1}H J-coupling spectral peaks at 4°C that are not present at RT. The next step will be the manufacturing of a ^{15}N, ^{13}C labelled wt-TTR, grown in ~99% deuterated water M9 medium, which will serve as a probe for triple resonance experiments that can include NHCA, HN(CA)CB and HN(COCA)CB, in order to assign the spectra at both temperatures. This type of experiment allows for assignment of ^{1}H-^{15}N HSQC spectra at both temperatures and therefore can give clear information in terms of what amino acids are dynamical or structural changes in the molecule.

To gain physiological relevance, future experiments should be performed at 37°C instead of RT.

In summary, we have successfully determined that conformational differences exist among wt-TTR purified and stored at 4°C compared to RT, which could explain cytotoxicity against human SH-SY5Y neuroblastoma cells. It is of extreme interest to determine exactly where in the molecule this conformational change occurs by the decrease in temperature. This information could possibly reveal the cytotoxic epitopes related to those displayed by the most toxic aggregates of wt-TTR. Knowledge about this epitopes could serve as future therapy targets. In order to determine whether cell toxicity is induced by the same epitope, a cellular study using the patch-clamp technique measuring ions flux could give further clue into whether the same cellular response is being induced.

5.- CONCLUSIONS

We have successfully produced and purified unlabeled wt-TTR for studies of denaturation kinetics followed by intrinsic tryptophan fluorescence. The recombinant wt-TTR preparations were molecular weight confirmed using MALDI-TOF mass spectrometry.

The denaturation kinetics experiment confirmed a higher tetramer dissociation rate at 4°C compared to RT, as previously determined for other temperature intervals.

Uniformly ^{15}N labeled wt-TTR grown in 99% D_2O M9 medium was successfully produced and purified, showing a high loss of deuterons from labile positions as judged from MALDI-TOF mass spectrometry measurements.

Finally, we were able to determine using NMR spectroscopy that conformational differences exist among wt-TTR purified and stored at 4°C and RT. The HXMS experiment did not show the expected differences among the two preparations, which could be due to a bad experimental design.

6.- REFERENCES

1. Anfinsen, C. B. Principles that Govern the Folding of Protein Chains (1973) *Science.* **181,** 223-230.
2. Dobson, C. M. Protein folding and misfolding (2003) *Nature* **426,** 884-889.
3. Hammarström, P. Protein folding, misfolding and disease (2009) *FEBS Lett.* **583**, 2579-2580.
4. Dobson, C. M. Getting out of shape (2002) *Nature* **418**, 729-730.
5. Hammarström, P. The bloody path of amyloids and prions (2007) *J. Thromb. Haemost.* **5**, 1136-1138.
6. Lindgren, M., Sörgjerd, K., Hammarström, P. Detection and characterization of aggregates, prefibrillar amyloidogenic oligomers, and protofibrils using fluorescence spectroscopy (2005) *Biophys J.* **88**, 4200-4212.
7. Mucke, L. Alzheimer's disease (2009) *Nature* **461**, 895-897.
8. Faller, P., Hureau, C. Bioinorganic chemistry of copper and zinc ions coordinated to amyloid-β peptide (2009) *Dalton Trans.* **21**, 1080-1094.
9. Stefani, M. Protein misfolding and aggregation: new examples in medicine and biology of the dark side of the protein world (2004) *Biochim. Biophys. Acta.* **1739**, 5-25.
10. Bhak, G., Choe, Y. J., Paik, S. R. Mechanism of amyloidogenesis: nucleation-dependent fibrillation versus double-concerted fibrillation (2009) *BMB Rep.* **42**, 541-551.
11. Lindgren, M., Hammarström , P. Amyloid oligomers: spectroscopic characterization of amyloidogenic protein states (2010) *FEBS J.* **277**, 1380-1388.
12. Trivella, D. B., Bleicher, L., Palmieri, L. D., Wiggers, H. J., Montanari, C. A., Kelly, J. W., Lima, L. M., Foguel, D., Polikarpov, I. Conformational differences between the wild type and V30M mutant transthyretin modulate its binding to genistein: Implications to tetramer stability and ligand-binding (2010) *J. Struct. Biol.* Accepted Manuscript.
13. Sörgjerd, K., Klingstedt, T., Lindgren, M., Kågedal, K., Hammarström, P. Prefibrillar transthyretin oligomers and cold stored native tetrameric transthyretin are cytotoxic in cell culture (2008) *Biochem. Biophys. Res. Commun.* **377**, 1072-1078.
14. Westermark P, Sletten K, Johansson B, Cornwell G. G. Fibril in senile systemic amyloidosis is derived from normal transthyretin (1990) *Proc. Natl. Acad. Sci. U. S. A.* **87**, 2843-2845.
15. Kabat, E. A., Moore, D. H., Landow, H. AN ELECTROPHORETIC STUDY OF THE PROTEIN COMPONENTS IN CEREBROSPINAL FLUID AND THEIR RELATIONSHIP TO THE SERUM PROTEINS (1942) *J. Clin. Invest.* **21,** 571-577.

16. Prapunpoj, P., Leelawatwattana, L. Evolutionary changes to transthyretin: structure-function relationships (2009) *FEBS J.* **276**, 5330-5341.

17. Hou, X., Aguilar, M. I., Small, D. H. Transthyretin and familial amyloidotic polyneuropathy. Recent progress in understanding the molecular mechanism of neurodegeneration (2007) *FEBS J.* **274**, 1637-1650.

18. Hamilton, J.A., Benson, M.D. Transthyretin: a review from a structural perspective (2001) *Cell. Mol. Life Sci.* **58**, 1491-1521.

19. Liu, K., Cho, H. S., Hoyt, D. W., Nguyen, T. N., Olds, P., Kelly, J. W., Wemmer, D. E. Deuterium-proton exchange on the native wild-type transthyretin tetramer identifies the stable core of the individual subunits and indicates mobility at the subunit interface (2000) *J. Mol. Biol.* **303**, 555-565.

20. Quintas, A., Vaz, D. C., Cardoso, I., Saraiva, M. J., Brito, R. M. Tetramer dissociation and monomer partial unfolding precedes protofibril formation in amyloidogenic transthyretin variants (2001) *J. Biol. Chem.* **276**, 27207-27213.

21. Benson, M. D., Kincaid, J. C. The molecular biology and clinical features of amyloid neuropathy (2007) *Muscle Nerve.* **36**, 411-423.

22. Lai, Z., Colón, W., Kelly, J. W. The acid-mediated denaturation pathway of transthyretin yields a conformational intermediate that can self-assemble into amyloid (1996) *Biochemistry* **35**, 6470-6482.

23. Liu, K., Cho, H. S., Lashuel, H. A., Kelly, J. W., Wemmer, D. E. A glimpse of a possible amyloidogenic intermediate of transthyretin (2000) *Nat. Struct. Biol.* **7**, 754-757.

24. Stangou, A. J., Hawkins, P. N., Heaton, N. D., Rela, M., Monaghan, M., Nihoyannopoulos, P., O'Grady, J., Pepys, M. B., Williams, R. Progressive cardiac amyloidosis following liver transplantation for familial amyloid polyneuropathy: implications for amyloid fibrillogenesis (1998) *Transplantation* **66**, 229-233.

25. Schneider, F., Hammarström, P., Kelly, J.W. Transthyretin slowly exchanges subunits under physiological conditions: A convenient chromatographic method to study subunit exchange in oligomeric proteins (2001) *Protein Sci.* **10**, 1606-1613.

26. Hammarström, P., Jiang, X., Deechongkit, S., Kelly, J. W. Anion shielding of electrostatic repulsions in transthyretin modulates stability and amyloidosis: insight into the chaotrope unfolding dichotomy (2001) *Biochemistry* **25**, 11453-11459.

27. Tsutsui, Y., Wintrode, P. L. Hydrogen/deuterium exchange-mass spectrometry: a powerful tool for probing protein structure, dynamics and interactions (2007) *Curr. Med. Chem.* **14**, 2344-2358.

28. Tugarinov, V., Choy, W. Y., Orekhov, V. Y., Kay, L. E. Solution NMR-derived global fold of a monomeric 82-kDa enzyme (2005) *Proc. Natl. Acad. Sci. U. S. A.* **102**, 622-627.

29. Felli, I. C., Brutscher, B. Recent advances in solution NMR: fast methods and heteronuclear direct detection (2009) *Chemphyschem.* **10**, 1356-1368

30. Hore, P. J. (1995) Nuclear Magnetic Resonance. 1st ed., Oxford: Oxford University Press.

31. Rule, G. S., Hitchens, T. K. (2006) Fundamentals of Protein NMR Spectroscopy. 1st ed., Volume 5., Dordrecht: Springer.

32. Keeler, J. (2005) Understanding NMR Spectroscopy. 1st ed., West Sussex: Wiley.
33. Chen, C., Smye, S. W., Robinson, M. P., Evans, J. A. Membrane electroporation theories: a review (2006) *Med. Biol. Eng. Comput.* **44**, 5-14.
34. PerSeptive Biosystems. Voyager™ Biospectrometry™ Workstation with Delayed Extraction™ Technology User's Guide. PerSeptive Biosystems, Inc., 1996.
35. Watson, J. T. (1997) Introduction to Mass Spectrometry. 3rd ed., Hardcover; Lippincott-Raven Publishers.
36. Lundström, P., Vallurupalli, P., Hansen, D.F., Kay, L.E. Isotope labeling methods for studies of excited protein states by relaxation dispersion NMR spectroscopy (2009) *Nat. Protoc.* **4**, 1641-1648.
37. Busso, D., Stierlé, M., Thierry, J. C., Moras, D. A comparison of inoculation methods to simplify recombinant protein expression screening in Escherichia coli (2008) *Biotechniques* **44**, 101-106.
38. Hammarström, P., Jiang, X., Hurshman, A. R., Powers, E. T., Kelly, J. W. Sequence-dependent denaturation energetics: A major determinant in amyloid disease diversity (2002) *Proc. Natl. Acad. Sci. U. S. A.* **99**, 16427-16432.
39. Hauge, C., Antal, T. L., Hirschberg, D., Doehn, U., Thorup, K., Idrissova, L., Hansen, K., Jensen, O. N., Jørgensen, T. J., Biondi, R. M., Frödin, M. Mechanism for activation of the growth factor-activated AGC kinases by turn motif phosphorylation (2007) *EMBO J.* **26**, 2251-2261.
40. Weis, D. D., Engen, J. R., Kass, I. J. Semi-automated data processing of hydrogen exchange mass spectra using HX-Express (2006*) J. Am. Soc. Mass. Spectrom.* **17**, 1700-1703.
41. Kavan, D., Man, P. MSTools-web based application for visualization and presentation of HXMS data (2010) *Int. J. Mass Spectrom.* 1387-3806.
42. Liang, M. P., Banatao, D. R., Klein, T. E., Brutlag, D. L., Altman, R. B. WebFEATURE: An interactive web tool for identifying and visualizing functional sites on macromolecular structures (2003) *Nucleic Acids Res.* **31**, 3324-3327.
43. Lundström, P. (2010) MWcalc software, Linköping (Not published).
44. Gardner, K. H., Kay, L. E. The use of 2H, 13C, 15N multidimensional NMR to study the structure and dynamics of proteins (1998) *Annu. Rev. Biophys. Biomol. Struct.* **27**, 357-406.
45. Kay, L. E., Keifer, P., Saarinen, T. Pure absorption gradient enhanced heteronuclear single quantum correlation spectroscopy with improved sensitivity (1992) *J. Am. Chem. Soc.* **114**, 10663–10665.
46. Nietlispach, D. Suppression of anti-TROSY lines in a sensitivity enhanced gradient selection TROSY scheme (2005) *J. Biomol. NMR* **31**, 161-166.
47. Goddard, T. D., Kneller, D.G. *SPARKY 3* (computer program) (2004) University of California, San Francisco.
48. Hammarström, P., Wiseman, R. L., Powers, E. T., Kelly, J. W. Prevention of transthyretin amyloid disease by changing protein misfolding energetic (2003) *Science* **299**, 713-716.
49. Zhang, Y. Protein and peptide structure and interactions studied by hydrogen exchange and NMR. Ph.D. Thesis, Structural Biology and Molecular Biophysics, University of Pennsylvania, PA, USA.

50. Bai, Y., Milne, J. S., Mayne, L., Englander, S. W. Primary structure effects on peptide group hydrogen exchange (1993) *Proteins*. **17**, 75-86
51. Billeter, M., Wagner, G., Wüthrich, K. Solution NMR structure determination of proteins revisited (2008) *J. Biomol NMR* **42**, 155-158.
52. Dill, K. A. Dominant forces in protein folding (1990) *Biochemistry* **29**, 7133-7155.
53. Paliy, O., Bloor, D., Brockwell, D., Gilbert, P., Barber, J. Improved methods of cultivation and production of deuteriated proteins from E. coli strains grown on fully deuteriated minimal medium (2003) *J. Appl. Microbiol.* **95**, 580-586.
54. Lee, B, Krishnanchettiara, S., Lateefa, S. S., Lia, C., Guptaa S. Random protein association analyses of MALDI-TOF mass spectra of two- and three-component protein systems using binomial and multinomial distribution (2006) *Int. J. Mass Spectrom.* **254**, 101-105.
55. Lai, Z., McCulloch, J., Lashuel, H. A., Kelly, J. W. Guanidine hydrochloride-induced denaturation and refolding of transthyretin exhibits a marked hysteresis: equilibria with high kinetic barriers (1997) *Biochemistry* **35**, 10230-10239.
56. Niraula, T. N., Haraoka, K., Ando, Y., Li, H., Yamada, H., Akasaka, K. Decreased thermodynamic stability as a crucial factor for familial amyloidotic polyneuropathy (2002) *J. Mol. Biomol.* **320**, 333-342.

8.- APPENDIX

A.- Cultivating broths:

SOB:

4 g Tryptone
1 g Yeast extract
0,1 g NaCl
Add dH$_2$O to a final volume of 200 mL and autoclave.
Before use, add SOC solution to SOB in a 1:100 ratio.

SOC:

10,81 g Glucose
6,10 g MgCl$_2$
7,39 g MgSO$_4$
Add dH$_2$O to a final volume of 30 mL.

LB medium:

To 900 mL of dH$_2$O add:

20 g Peptone
20 g NaCl
10 g Yeast extract
Add dH$_2$O to a final volume of 1 L and autoclave.

LB agar plates:

To 900 mL of dH$_2$O add:

15 g Agar
20 g Peptone
20 g NaCl
10 g Yeast extract
Add dH$_2$O to a final volume of 1 L and autoclave.

Add antibiotics to the LB agar before it is poured into petri plates.

D$_2$O M9 medium:

To prepare 1 L add:

6 g Na$_2$HPO$_4$
3 g KH$_2$PO$_4$
0,5 g NaCl
0,5 g ^{15}NH$_4$Cl
246 mg MgSO$_4$ (pentahydrate)
10 mL vitamin sock solution
15 mg CaCl$_2$ (dihydrate)
0,04% (w/v) glucose
0,1 mg/mL carbenicillin
Add D$_2$O to a final volume of 1L and adjust pH to 7,4
Take 100 mL from this 1L medium and add 100 µL LB to start the first 100 mL culture.

B.- SDS-PAGE and Coomassie staining

SDS cocktail:

To 50 mL total volume add:

4,6 g DTT
6 g SDS
0,5 g Bromo phenyl blue
87% glycerol to up to a 50 mL volume

SDS-PAGE running buffer:

3 g Tris base
1 g SDS
14 g Glycine
Add dH$_2$O up to a final volume of 1 L

Separation gel:

4 mL 33% acrylamide
1,4 mL 1% bisacrylamide
2 mL 2,122M Tris-HCl pH 9,18 buffer

1,4 mL dH$_2$O
200 μL 5% (w/v) APS (ammonium persulfate)
23 μL TEMED

Concentration gel:

1,25 mL 33% acrylamide
2,5 mL 1% bisacrylamide
1,25 mL 0,5421M Tris-HCl pH 6,1 buffer
4,8 mL dH$_2$O
200 μL 5% (w/v) APS (ammonium persulfate)
20 μL TEMED

Coomassie stain:

To prepare 1 L total volume add:

1,25 g of Coomassie Brilliant Blue R-250
450 mL methanol
92 mL acetic acid
Add dH2O up to a final volume of 1 L

Destaining solution:

To 5 L total volume add:

0,5 L Acetic acid
2 L Methanol
2,5 L H$_2$O

Gel storage solution:

20% Ethanol
5% Glycerol